Ocean Dynamics (2016) 66:461–482
DOI 10.1007/s10236-016-0926-2

Numerical study of tides in Ontario Lacus, a hydrocarbon lake on the surface of the Saturnian moon Titan

David Vincent[1] · Özgur Karatekin[2] · Valentin Vallaeys[1] · Alexander G. Hayes[3] · Marco Mastrogiuseppe[4] · Claudia Notarnicola[5] · Véronique Dehant[2,6] · Eric Deleersnijder[7,8]

Received: 14 October 2015 / Accepted: 22 January 2016 / Published online: 7 March 2016

Abstract In the context of the emergence of extra-terrestrial oceanography, we adapted an existing oceanographic model, SLIM (www.climate.be/slim), to the conditions of Titan, a moon of Saturn. The tidal response of the largest southern lake at Titan's surface, namely Ontario Lacus, is simulated. SLIM solves the 2D, depth-averaged shallow water equations on an unstructured mesh using the discontinuous Galerkin finite element method, which allows for high spatial resolution wherever needed. The impact of the wind forcing, the bathymetry, and the bottom friction is also discussed. The predicted maximum tidal range is about 0.56 m in the southern part of the lake, which is more than twice as large as the previous estimates (see Tokano, Ocean Dyn 60:(4) 803–817 doi:10.1007/s10236-010-0285-3 2010). The patterns and magnitude of the current are also markedly different from those of previous studies: the tidal motion is not aligned with the major axis of the lake and the speed is larger nearshore. Indeed, the main tidal component rotates clockwise in an exact period of one Titan day and the tidal currents can reach 0.046 ms^{-1} close to the shores depending on the geometry and the bathymetry. Except for these specific nearshore regions, the current speed is less than 0.02 ms^{-1}. Circular patterns can be observed offshore, their rotational direction and size varying along the day.

Keywords Ontario Lacus · Tides · Titan · Finite element · Numerical model · Extraterrestrial oceanography

Responsible Editor: Dirk Olbers

✉ D. Vincent
david.vincent@uclouvain.be

1 Institute of Mechanics, Materials and Civil Engineering (IMMC), Université catholique de Louvain, 4 Avenue Georges Lemaître, 1348 Louvain-la-Neuve, Belgium

2 Royal observatory of Belgium, 3 Avenue Circulaire, 1180 Bruxelles, Belgium

3 Cornell Center for Astrophysics and Planetary Science, Cornell University, 412 Space Sciences Building, Ithaca, NY 14853, USA

4 Cornell Center for Astrophysics and Planetary Science, Cornell University, 410 Space Sciences Building, Ithaca, NY 14853, USA

5 Institute for Applied Remote Sensing, EURAC, Bolzano, Italy

6 Earth and Life Institute (ELI), Université catholique de Louvain, 2 Croix du Sud, 1348 Louvain-la-Neuve, Belgium

7 Institute of Mechanics, Materials and Civil Engineering (IMMC) & Earth and Life Institute (ELI), Université catholique de Louvain, 4 Avenue Georges Lemaître, 1348 Louvain-la-Neuve, Belgium

8 Delft Institute of Applied Mathematics (DIAM), Delft University of Technology, Mekelweg 4, 2628CD Delft, The Netherlands

1 Introduction

Titan, Saturn's largest moon, is the only celestial body of the solar system, other than the Earth and Mars, that has a substance, methane in this case, present in the solid, liquid, and gaseous states at its surface. The presence of liquids on its surface was evoked following Earth-based observations and Voyager's flyby in 1980 (see, e.g., Hanel et al.

1981; Samuelson et al. 1981). The *Cassini* spacecraft, which has been observing the Saturnian system since 2004 and is now in its extended mission named *Solstice*, and its probe *Huygens* have shown the existence of a methane cycle on Titan similar to the hydrological cycle on Earth. *Cassini* first detected liquid bodies in the southern polar region of Titan surface in 2004 by means of the imaging science subsystem[1] (ISS) (McEwen et al. 2005). Its Radar[2] showed dark patches, interpreted as lakes, in the northern polar region in 2006 (Stofan et al. 2007). These seas[3] and lakes are asymmetrically distributed with respect to the equator (Aharonson et al. 2009): there are much more lakes in the northern latitudes, where they are larger and deeper (Hayes et al. 2008). These liquid bodies are mainly composed of methane with ethane, nitrogen, and other low-molecular-mass hydrocarbons (see, e.g., Brown et al. 2008; Cordier et al. 2009; Glein and Shock 2013; Mastrogiuseppe et al. 2014; Luspay-Kuti et al. 2015; Mitchell et al. 2015; Tan et al. 2013, 2015). The estimated composition is established with the help of these models (see Section 2.2) and can vary from one lake to another.

The study of such lakes and seas belongs to a new scientific research field usually referred to as *extra-terrestrial oceanography*. Indeed, although the governing equations are similar to those of terrestrial oceanography, there are significant differences that need to be taken into account: extra-terrestrial surface seas or lakes involve regimes of temperature, pressure, composition, and physical environment (gravity, tidal forces, rotational and orbital periodicities, etc.) that are not observed in Earth's oceans. In order to study the dynamics of surface lakes and seas of Titan, we adapt consequently `SLIM` (www.climate.be/slim), an Earth-based model developed at Université catholique de Louvain, to Titan environment. This model solves the 2D depth-averaged shallow water equations using the discontinuous Galerkin finite element method.

In this work, we focus on one of Titan's lakes: Ontario Lacus. It is the largest lake in the southern hemisphere (with its center at 72° S, 175° E.), covering approximately an area of 200 × 70 km (Wall et al. 2010). Since its discovery, Ontario Lacus has been the subject of several publications focusing on morphology (Wall et al. 2010; Cornet et al. 2012), composition (Brown et al. 2008), bathymetry (Hayes et al. 2010; Ventura et al. 2012; Hayes 2016), as well as tides (Tokano 2010). Differences between ISS images taken in 2005 (Rev009, $L_s = 306°$)[4] and in 2009 (T51, $L_s = 355°$) suggested possible shoreline variations (Turtle et al. 2011). Synthetic aperture radar (SAR) images from 2009 (T57, $L_s = 358°$ and T58, $L_s = 359°$) (see Wall et al. 2010; Hayes et al. 2011) gave additional support to the hypothesis of seasonal variations in lake volume and shorelines. Evaporation and/or infiltration of surface liquid could be responsible for such variations (Lunine et al. 2009; Turtle et al. 2011). Indeed, those observations took place during the southern summer, when evaporation was predicted to be the greatest. However, due to their low resolution, analysis of ISS images could not be conclusive and the existence of seasonal shoreline variations remained questionable (Cornet et al. 2012). Indeed, subsequent SAR images (T65 in 2010, $L_s = 5.5°$) did not observed any indications for shoreline changes in comparison with 2009 images. Nevertheless, in the present study, shoreline variations due to the tides are briefly discussed.

The first pieces of information about Ontario Lacus bathymetry came from T49, T57, and T58 observations (2008 and 2009) which were used by Hayes et al. (2010) to derive the bathymetry near the shoreline. Using SAR data from T65, Ventura et al. (2012) estimated the bathymetry over the whole lake. Their results indicate a maximum depth of about 30 m for a data map resolution of 256 pix/deg (i.e., about 0.17 km/pix). The most recent work from the Cassini radar team suggests that the lake could be even deeper than predicted by Ventura et al. (2012) (see Hayes et al. 2016 and Mastrogiuseppe 2016, Radar Bathymetry and Composition of Titan's Ontario Lacus from waveform inversion of Cassini altimetric data, will be soon submitted to Icarus). In this study, we consider all of above-mentioned bathymetries and quantify their influence on the tidal response. Besides the bathymetry, there are several other parameters that are not well known such as the exact lake composition and the roughness of Ontario Lacus bottom. We will also quantify their influence on the tidal response. Finally, due to the lack of direct wind observations above the lake, the sensitivity to the wind forcing will be investigated for some hypothetical scenarios. To these ends, the 2D depth-averaged shallow water equations are solved on unstructured meshes with a spatial resolution ranging from 1 to 5 km. This would allow for a precise implementation of Ontario Lacus coastline and bathymetries, and a better representation of small-scale phenomena than previous studies.

Various aspects of the tides of the surface seas and lakes of Titan have been the subject of previous studies. Sagan and Dermott (1982) and Dermott and Sagan (1995) constructed the appearance of Titan's surface (which was

[1]Imaging Science Subsystem: it takes pictures in visible, near-ultraviolet, and near-infrared light. (see Porco et al, 2004).

[2]Radar: it maps the surface of Titan using a radar imager to pierce the veil of haze. It is also used to measure heights of surface features. The synthetic aperture radar observed Titan in 13.78 GHz Ku-band with a resolution ranging from 0.35 to 1.7 km (see Elachi et al, 2004).

[3]The largest lakes are referred to as seas (Mare) and the others as lakes (Lacus), according to the nomenclature of the International Astronomical Union. It only reflects the size of the lake.

[4]The true anomaly of Titan, L_s, is the angle between the direction of the perikron and the current position of Titan as seen from Saturn.

unknown at that time) by conducting analyses of theoretical global surface ocean and disconnected seas and lakes on Titan's surface. Tokano (2010) discussed the tidal responses of Ontario Lacus and Kraken Mare while Tokano et al. (2014) and Tokano and Lorenz (2015), respectively, studied the tides and the surface stress response in the northern seas. On the other hand, Sears (1995) and Lorenz et al. (2014) studied the tidal dissipation. In order to simulate the tides in Ontario Lacus, Tokano (2010) used a 3D hydrostatic, baroclinic ocean circulation model. The only forcing taken into account was the astronomical forcing due to Saturn. He computed the surface displacement, the velocity field, and the temperature. He used a structured grid with a spatial resolution of 10 km and, due to the lack of information at that time, a constant depth of 20 m.

The numerical model developed has two purposes. The first one is specific to the surface lakes and seas of Titan: it allows us to discuss their tidal response. Understanding the tides is important in itself but also for explaining potential transient events in Titan's seas, for understanding the currents and for planning future missions. Such pieces of information may improve Cassini data analysis as well. The second one is more general: it could be used for other extra-terrestrial oceans, seas, and lakes.

This paper is organised as follows. Section 2 deals with Ontario Lacus environment and characteristics: atmospheric conditions, lake composition, and bathymetries are described. Section 3 presents the model, SLIM, the forcings applied, and the meshes. In Section 4, a reference case is studied and will be used as a basis for sensitivity analyses to bottom friction, bathymetry, and wind. Our results are discussed and compared with previous ones in Section 5, and conclusions are drawn in Section 6.

2 Ontario Lacus environment and characteristics

Ontario Lacus was flown over at least twice by each Cassini instrument (complete or partial flybys): ISS in 2004, 2005, and 2009, VIMS[5] in 2007 and 2009, and Radar in 2009 and 2010. It has the shape of a right footprint (see Fig. 1) and is named after Lake Ontario (one of the Great Lakes of North America). It is connected to a hydrological network (for example, in area N on Fig. 1) (Wall et al. 2010; Cornet et al. 2012) which can provide liquid hydrocarbons during and after precipitations. Several, quite different, morphologies were observed along the shoreline of Ontario Lacus: deeply incised bays, mountainous region, beaches... (see Wall et al. 2010; Cornet et al. 2012 for further details).

[5]Visible and Infrared Mapping Spectrometer: it identifies the chemical compositions of the surfaces, atmospheres, and rings of Saturn and its moons by measuring colors of visible light and infrared energy emitted or reflected (Brown et al. 2004).

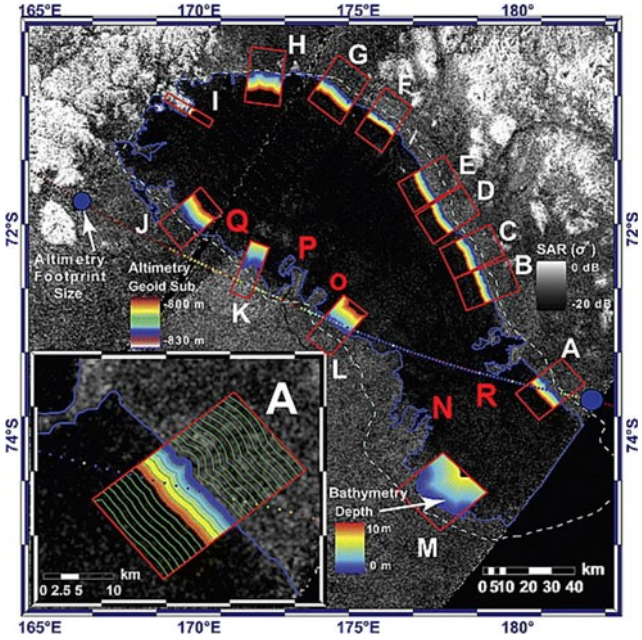

Fig. 1 Map of Ontario Lacus. Letters from *A* to *M* show the study areas of Hayes et al. (2010) which derived a nearshore bathymetry in these regions. The *red letters*, from *N* to *R*, are used in this article to refer to particular areas (adapted from www.titanexploration.com; original image credit: Cassini Radar Science team, NASA/JPL/Caltech)

2.1 Atmospheric conditions

The atmosphere is mainly composed of nitrogen with a small amount of methane and a still smaller amount of other species (e.g., ^{40}Ar, ^{36}Ar, cyanogen, ethane) (Niemann et al. 2005) (for detailed composition, see Table 1 in Cordier et al. (2009)).

The only in situ measurements of Titan atmospheric conditions were provided by the Huygens probe at its landing site. Nevertheless, Titan surface temperature has also been inferred from the CIRS[6] far infrared spectra collected from 2004 (right after the northern winter solstice) to 2008 (late northern winter) by Jennings et al. (2009) and from 2004 to 2010 (in the early northern spring) by Cottini et al. (2012). Their results are consistent with each other and with Huygens measurements (see Fulchignoni et al. 2005). Seasonal variations were observed by both authors. Jennings et al. (2009) did not take into account the diurnal changes while Cottini et al. (2012) observed that the diurnal features disappeared at latitudes greater than 20–30° in the north and 30–40° in the south. Nevertheless, they took into account neither the data from latitudes greater than 60° nor the local influence of the lake. According to Jennings et al. (2009), during the northern winter, the temperature at Ontario Lacus

[6]Composite Infrared Spectromter : it measures infrared energy from the surfaces, atmospheres, and rings of Saturn and its moons to study their temperature and compositions (Flasar et al. 2004).

latitude (72° S) is more than 1 K lower than at the equator (93.56 K) while, at 72° N, it is more than 2 K lower than at the equator. Tan et al. (2015) established a formula describing the surface temperature as a function of the latitude and the time from January 2005 to December 2013 from Jennings et al. (2011) and Cottini et al. (2012) temperature profiles. The surface temperature variations between the northern and the southern end of Ontario Lacus (respectively 70° S and 74° S) are minimum (about 0.14 K) in January 2005 and increase almost linearly to reach about 0.26 K in December 2013. The temperature in the middle of the lake (at 72° S) is about 92.7 K in January 2005 and decreases almost linearly to reach about 90.3 K in December 2013. These absolute values have to be used with caution: the results do not take into account the local influence of the lake on the temperature (no variation as a function of the longitude was taken into account).

Due to the lack of in situ measurements for atmospheric pressure, precipitations, and winds, models had to be used to predict these fields: several global circulation models (GCMs) were proposed (e.g., Tokano 2008, 2009; Friedson 2009; Lebonnois 2012; Schneider 2012). According to these GCMs, the atmospheric pressure variations are small at the surface and the winds are subject to significant spatial, seasonal, and diurnal variations. Additionally, the wind speed may vary depending on the lake composition: if the seas are methane rich, the wind speed could be different than for ethane-rich seas (Tokano 2009; Lorenz et al. 2012). The tidal wind has neither a preferential direction nor a specific time distribution while the wind due to the convergence of moist air over the lake area is directed offshore and can be stronger than the tidal wind (Tokano 2009). The predicted wind speed ranges from 0 to 2 ms^{-1} according to the location and the season (Lorenz et al. 2012; Lorenz 2013). In view of the results obtained by means of the GCMs, we choose to discuss the response of Ontario Lacus to four hypothetical strong winds which are consistent with GCMs prediction in terms of magnitude (see Section 4.3). Indeed, there are uncertainties about the lake composition (see Section 2.2) which could influence the wind speed and the local orientation of the wind is uncertain. Moreover, each of these models uses simplifying assumptions and none of them is fully consistent with observations (Schneider et al. 2012). Furthermore, we choose to study Ontario Lacus tidal response on a short period of time (1 Titan day (TD)) while the results published in the literature are on a long period (1 Titan year, i.e., 29.7 Earth years). For the same reasons, the atmospheric pressure gradient, the precipitations and the methane evaporation are not taken into account. An accurate study of the wind, precipitation, and evaporation impact on Ontario Lacus would require a mesoscale atmospheric model and a longer study period but this is beyond the scope of this article.

2.2 Ontario Lacus composition

Liquid ethane was identified in Ontario Lacus in 2008 by Brown et al. (2008) while the identification of liquid methane on Titan's surface is made difficult by the presence of methane in the atmosphere. In the absence of in situ measurements, a detailed composition of lakes was modeled by Cordier et al. (2009), Tan et al. (2013, 2015), and Glein and Shock (2013) while Luspay-Kuti et al. (2015) computed a rough approximation of Ontario Lacus composition from experimental evaporation rates. Cordier et al. (2009) and Tan et al. (2013, 2015) distinguished two types of lakes: the near-equator lakes and the high latitudes lakes. This distinction is the result of the temperature difference between the equator and the high latitudes. Ontario Lacus belongs to the second category.

Cordier et al. (2009) established the composition by considering the lakes as non ideal solutions in thermodynamic equilibrium with the atmosphere. Nevertheless, this model is quite sensitive to uncertainties about thermodynamic data and other parameters: the relative standard deviations remain between 10 and 300 % according to the species considered (Cordier et al. 2012). Tan et al. (2013) also considered this equilibrium and used an equation of state to model the chemical system of the atmosphere. Tan et al. (2015) used the same model as Tan et al. (2013) and included the effect of multicomponent mixtures. Glein and Shock (2013) developed a van Laar model parameterized by using experimental phase equilibrium data. Luspay-Kuti et al. (2015) deduced a composition by comparing experimental evaporation rates and that computed by Hayes et al. (2011) to explain the shoreline variations.

Cordier et al. (2009) and Luspay-Kuti et al. (2015) predicted an ethane-rich composition while Tan et al. (2013, 2015) predicted a methane-rich one. Nevertheless, Tan et al. (2015) predicted that the composition will vary seasonally: the liquid would have more ethane and other heavy components in winter than in summer. Glein and Shock (2013) also predicted a methane-rich composition but their results significantly vary with the mixing ratio of methane. If the mixing ratio of methane suggested by Voyager 1 was used, they would obtain an ethane-rich lake.

According to Mastrogiuseppe et al. (2014) and LeGall et al. (2015, Composition, seasonal change and bathymetry of Ligeia Mare, Titan, derived from its microwave thermal emission submitted to Journal of Geophysical Research-Planet), the dominant component of the lake can also be identified from the dielectric constant and the loss tangent[7] of the liquid. Using these observations, LeGall et al.

[7]The loss tangent is the tangent of the loss angle. It is used to parametrise the electromagnetic energy dissipation inherent to a dielectric material.

(2015, submitted) predicted that Ligeia Mare is methane-rich. However, it does not imply that Ontario Lacus is methane-rich. Indeed, according to Glein and Shock (2013), higher temperatures cause liquid to lose methane and nitrogen and to gain ethane. CIRS measurements suggest that, at least during the summer, the lakes at 70° S (like Ontario Lacus) are about 1 K warmer than those at 70° N (Ligeia Mare is about 77° N) (Jennings et al. 2009). Using the value of loss tangent derived by Mastrogiuseppe et al. (2015, Turning the Cassini RADAR into a sounder to probe the depth and composition of Titan's seas through Monte Carlo based modeling of altimetry waveforms, submitted to IEEE), Hayes (2016) predicted a composition of 47 % CH_4, 40 % C_2H_6, and 13 % N_2.

The chemical models result in a liquid of similar density but there are some significant differences about the molecular viscosity: that predicted by Cordier et al. (2009) and Luspay-Kuti et al. (2015) are larger than that predicted by Tan et al. (2013) (respectively by a factor of 5 and up to 3). The lake also carries some solid particles like acetylene and high molecular weight organics produced by atmospheric photochemistry (see, e.g., Lorenz et al. 2010, 2011; Lorenz 2013) (Tan et al. 2013 showed that tholins and acetylene could be present in Titan lakes). These particles modify the lake properties. Thus density and viscosity cannot be accurately derived from the lake composition.

Among these compositions, that of Cordier et al. (2009) will be adopted as a baseline: for a temperature of 90 K, Cordier et al. (2009)'s composition[8] results in a density of 662 kg/m^3 and a viscosity of 1736×10^{-6} Pa s according to Lorenz et al. (2010). The impact of the lake composition will later be shortly discussed in terms of molecular viscosity and density within the range given by the above-mentioned models (i.e., a density ranging from 547 to 662 kg/m^3 and a molecular viscosity ranging from 200×10^{-6} to 2000×10^{-6} Pa s).

2.3 Bathymetry

An important ingredient of the model of Ontario Lacus is the bathymetry. Presently, bathymetries are available for a few lakes/seas: Ontario Lacus (see Ventura 2012; Hayes 2016 and Mastrogiuseppe 2016, soon submitted to Icarus), Ligeia Mare (see Mastrogiuseppe 2014), and Kraken Mare (see Lorenz et al. 2014). This last one is computed from an empirical rule observed in Earth lakes basin and adapted to Titan seas from Ligeia Mare measured bathymetry.

Ventura et al. (2012) derived Ontario Lacus' bathymetry from the SAR data of the T65 flyby (January 12, 2010) using two approaches for backscattering description: a simplified semi-empirical model and a physically based one. Both methods rely on composition and seabed scattering properties and they return different results according to parameters such as the wind speed for the latter and the surface scattering for the former. In this work, we use the bathymetry returned by the second method with a wind speed of 0.7 ms^{-1} which results in a maximum[9] and a mean depths of respectively 28 and 9.67 m (see Fig. 2a). The methodology used to derive this bathymetry is a combination of electromagnetic modelling and Bayesian approach to perform the inversion and obtain from SAR backscattering values the lake optical thickness. The conversion to physical depth is then obtained by using the loss tangent value as calculated in Hayes et al. (2010). This is the result which shows less extreme values and which best meets the nearshore results obtained by Hayes et al. (2010). We obtain the implemented bathymetry of Fig. 2a by homogenising the physical depth in order to be coherent with the observed smoothness of bottom of dry lakes. It will be referred to as *bathy A*.

The second bathymetry, namely *bathy B*, is obtained by extending the nearshore bathymetry predicted by Hayes et al. (2010) (see Fig. 2b). It is the most accurate bathymetry in the region close to the shore (<15 km) but the offshore depths are given by an extrapolation of the nearshore slopes, which is inaccurate far from the shore. Consequently, we will use *bathy B* to discuss the influence of the nearshore bathymetry and not to predict the tidal response of Ontario Lacus. Hayes et al. (2010) estimated the depth of the lake nearshore from the local topography slopes obtained by means of the radar altimetry profile. This partial bathymetry is then used to determine the nearshore (i.e., <15 km) imaginary component of the liquid complex index of refraction from SAR data of Titan flybys T57, T58, and T65 and altimetry observations (T49, $L_s = 352°$) (Hayes et al. 2010). Once the complex refractive index is known, it is used to estimate the local bathymetry slopes assuming uniform refractive properties throughout the lake (Hayes et al. 2010). *bathy B* is then obtained by extrapolating the mean bathymetry slopes presented in table 1 of Hayes et al. (2010) (see also Fig. 1). The maximum and mean depths obtained are respectively 49.8 and 15.8 m. The bathymetry map has the same shape as in *bathy A* but the maximum depth is larger and is not located at the same place than with *bathy A*. Due to its derivation, this bathymetry is much smoother than the two others.

The third bathymetry is also derived from SAR data. The Cassini Radar altimeter data from flyby T49 (December 21, 2008) were used to calibrate the SAR backscatter

[8]This composition is shown in Table 3 of Cordier et al. (2009). The main constituents and their lake mole fraction are C_2H_6 (7.64×10^{-1}), CH_4 (9.69×10^{-2}), C_3H_8 (7.42×10^{-2}), C_4H_8 (1.39×10^{-2}), N_2 (4.9×10^{-3}), Ar (5.01×10^{-6}), CO (4.21×10^{-7}), and H_2 (3.99×10^{-11}).

[9]In this paper, the words "maximum depth" refer to the maximum depth of the implemented bathymetry and not the maximum depth on the lake which is a function of the resolution of the data.

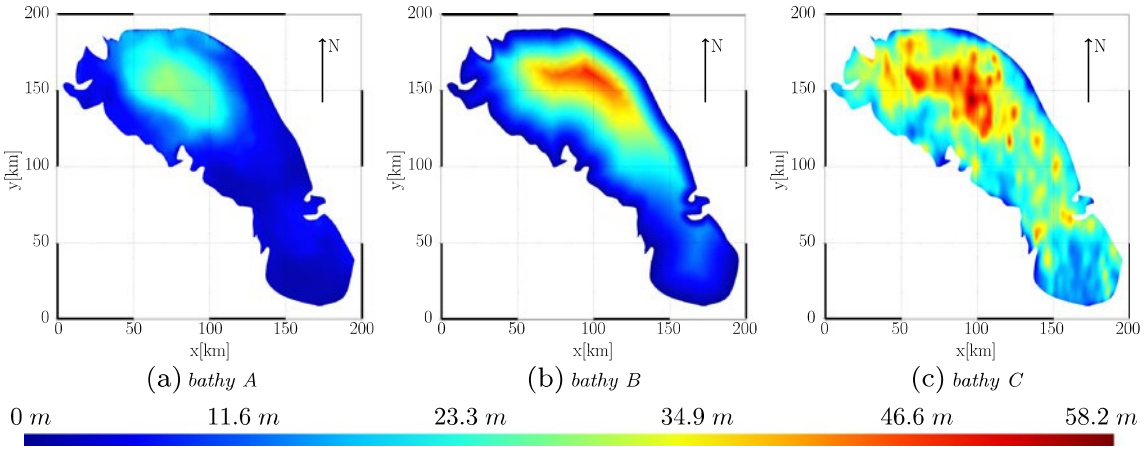

Fig. 2 Bathymetries of Ontario Lacus (in meters). Panel (**a**) is the bathymetry computed by Ventura et al. (2012) from SAR data. The bathymetry is smoothed to be coherent with the bottom of dry lakes. *bathy B* is shown in panel (**b**) and *bathy C* is shown in panel (**c**). Except at the shore, *bathy C* is deeper and presents more pits than *bathy A*. *bathy B* is also deeper than *bathy A* and is more accurate nearshore than *bathy C*

(for further information about this method, see Hayes et al. 2014). Nevertheless, the T49 pass was the first over a liquid body on Titan and the default attenuator settings were overwhelmed. Consequently, Mastrogiuseppe et al. (2015, submitted to IEEE) designed a model to recover the depths and absorptivity estimations in some saturated area. The depths across the lake are then extrapolated from the SAR data. The bathymetry obtained is shown in Hayes (2016). Describing this method in detail is the aim of a series of forthcoming publications. This method is different from that of Ventura et al. (2012): instead of a model, an extrapolation method is resorted to for the derivation of the bathymetry. The results are consistent with the direct depths measured by altimetry from T49 flyby (see Mastrogiuseppe et al. 2015, submitted to IEEE) but it is less accurate nearshore than *bathy B*. The implemented bathymetry is obtained by smoothing these data. This bathymetry will be referred to as *bathy C* (see Fig. 2c). The maximum and mean depths obtained are respectively 58.2 and 27.3 m, which is the same order of magnitude as with *bathy B* but is twice deeper than that predicted by Ventura et al. (2012). The deepest pit is located in the same region as in *bathy A* and *bathy B* but there are other smaller pits distributed over the lake (the small yellow/red spots offshore (it corresponds with the dark grey spots on a black and white copy)[10] which are not observed in *bathy A* and *bathy B*). *bathy C* is deeper than *bathy A* everywhere in the lake except at the shore: the dark blue areas (it corresponds with the dark areas on a black and white copy) nearshore are shallower. The bathymetry gradient offshore is more significant than in *bathy A* and *bathy B*.

3 Method

The model adapted to Titan conditions is introduced in Section 3.1. The tidal forcing applied is described in Section 3.2 and the various meshes used are briefly described in Section 3.3.

3.1 Model

The state-of-the-art numerical model used is the Second-generation Louvain-la-Neuve Ice-ocean Model (`SLIM`, www.climate.be/slim). It relies on the discontinuous Galerkin finite element method (DGFEM) to solve the 2D depth-averaged shallow water equations (see Eq. 1) on an unstructured mesh. The elevation, the velocity field, and their spatial derivatives are discretised by means of the DGFEM. The numerical solution is thus a piecewise polynomial function that can be discontinuous at the element interfaces. The inter-element fluxes are evaluated by means of an approximate Riemann solver (for further details, see Bernard et al. 2007). The time-marching scheme used is an implicit Runge-Kutta scheme using a Newton-Raphson solver allowing for a time step of the order of a thousandth of a Titan day ($\simeq$1378 s) to be used. Explicit schemes would request a time step of about 40 s, which would considerably slow down the simulation even with multi-rate schemes (for further details about multirate schemes, see Seny et al. 2013). This method is well-suited for advection-dominated problems as characteristics variables

[10]For interpretation of the references to color, the reader is referred to the web version of this article.

are upwinded across the element interface and does not suffer excessive numerical dissipation or oscillations. Moreover, it is highly parallelisable, local mass conservation is ensured and a wetting-drying algorithm, which will be used to deal with the tidal flats, is implemented (see Kärnä et al. 2011). Another asset of this method is the use of unstructured grids. Indeed, such grids allow the user to refine the mesh at some particular places (for example, in the vicinity of the shores or where the bathymetry gradient is the most significant, see Section 3.3) without significantly increasing the computational cost. SLIM has already been successfully used to simulate the tides in various terrestrial domains including the Scheldt estuary (e.g., De Brye et al. 2010), the Mahakam delta (e.g., De Brye et al. 2011), and the whole Great Barrier Reef (e.g., Lambrechts et al. 2008b). Preliminary work to adapt SLIM to extra-terrestrial environment has been done and it is now used to simulate liquid tides on Titan.

The 2D depth-averaged shallow water equations derive from the general mass and momentum conservation equations. The main assumptions are mentioned below. First, we assume a constant density. Tan et al. (2015) predicted a maximum liquid density variation due to temperature changes of about 50 kg/m^3 for the temperature variations observed between 2006 and 2013 by Jennings et al. (2009, 2011), and by Cottini et al. (2012). According to Cottini et al. (2012), the temperature diurnal variation are disappearing at latitudes greater than 40° S. Ontario Lacus being located near 72° S and the tidal time scale being much smaller than that of the temperature variations observed by Jennings et al. (2009, 2011), and by Cottini et al. (2012), the assumption that the density is constant can be resorted to. Second, Ontario Lacus maximum depth is about 58 m (*bathy C*) which is much smaller than the horizontal length scales. Thus, the aspect ratio is small implying that the hydrostatic assumption is valid. By integrating the equations vertically, one obtains Equations 1 (the atmospheric pressure gradient is neglected as we focus on the tidal response of the lake).

$$\begin{cases} \frac{\partial \boldsymbol{u}}{\partial t} + \boldsymbol{u}\cdot\nabla\boldsymbol{u} + f\boldsymbol{e}_z \wedge \boldsymbol{u} + g\nabla\eta \\ \quad = \frac{1}{H}\nabla\cdot(H\nu\nabla\boldsymbol{u}) + \frac{\boldsymbol{\tau}^s - \boldsymbol{\tau}^b}{\rho H} + \boldsymbol{S} \\ \frac{\partial \eta}{\partial t} + \nabla\cdot(H\boldsymbol{u}) = 0 \end{cases} \tag{1}$$

where $\boldsymbol{u}$ is the depth-averaged velocity; ∇ is the horizontal del operator; $f = 2\Omega\sin\phi \approx 8.67\times10^{-6}$ s^{-1} is the Coriolis parameter ($\Omega = 4.5601\times10^{-6}$ is Titan's orbital angular velocity and ϕ is the latitude); $\boldsymbol{e}_z$ is a unit vector pointing upwards in the local non-inertial cartesian basis; $g = 1.352$ ms^{-2} is the mean gravitational acceleration at Titan's surface; η is the surface elevation (positive upward); $H = h + \eta$ is the total liquid depth of the lake where h is the reference height of the water column; ρ is the density; ν is the horizontal eddy viscosity; $\boldsymbol{\tau}^s$ is the wind induced surface stress; $\boldsymbol{\tau}^b$ is the bottom stress; and $\boldsymbol{S}$ is the astronomical forcing term described in the following section.

We use the Smagorinsky's closure model to represent the eddy viscosity (Smagorinsky 1963) and an empirical Earth-based model, Chézy-Manning-Strickler's formulation (see, e.g., Lambrechts et al. 2008b), for bottom friction. Chézy-Manning-Strickler's formulation is:

$$\boldsymbol{\tau}^b = \rho g\mu^2 \frac{|\boldsymbol{u}|\boldsymbol{u}}{H^{1/3}} \tag{2}$$

where $\mu \in [0.01, 0.05]$ $sm^{-1/3}$ is Manning's roughness coefficient (it is set to 0.03 $sm^{-1/3}$ for the reference case, which corresponds to natural river bottom on Earth, and a sensitivity analysis will be conducted with respect to μ (see Section 4.2.2)).

There are some significant differences between the Earth and Titan: the liquid properties and behavior are different, the Coriolis term is smaller, the tidal forcing is larger than that due to the Sun and the Moon on Earth, and the mean gravitational acceleration is more than seven times smaller than on Earth. Some of these differences can be shown by means of the Rossby number $Ro = \frac{U}{fL_h}$ and the temporal Rossby number $Ro_t = \frac{1}{fT}$ (see Table 1) where f is the Coriolis parameter, $U \approx 10^{-2}$ ms^{-1} is the velocity scale predicted by our model, $L_h \approx 10^5$ m is the horizontal length scale, and T = 1 TD is the time scale. Local Titan's rotation time scale f^{-1} is smaller than the advective time scale $\frac{L_h}{U}$, in a similar way to what is observed in Lake Ontario and in Earth's oceans. It is also smaller than the time scale, which is not the case in Earth's oceans or in Lake Ontario.

Table 1 Rossby (Ro) and temporal Rossby (Ro$_t$) numbers of Ontario lacus, Lake Ontario, and Earth's oceans

	Ro	Ro_t
Ontario Lacus	3×10^{-2}	0.08
Lake Ontario[a]	5×10^{-2}	3.4
Earth oceans[b]	$\mathcal{O}(10^{-3})$	$\mathcal{O}(1)$

[a]The observed speed is used to compute Ro (i.e., the wind and the barometric pressure changes are partially responsible for these currents)

[b]For the M2 tide (principal lunar semi-diurnal tidal component) at mid-latitudes

3.2 Forcings

The astronomical forcings taken into account to compute the tidal response are those due to Saturn: the solar gravitational tide and the tides due to other planets and moons are neglected (Sagan and Dermott 1982). For instance, there is a ratio of $\mathcal{O}(10^{-6})$ between the solar potential and those taken into account herein. The remaining forcings are Titan's obliquity and its orbital eccentricity. Therefore, the tidal period is exactly 1 TD and the tidal cycle exhibits no spring-neap tide cycle.

The forcing is obtained from the horizontal gradient of the tidal potential. The latter is given by the sum of two contributions: the potential due to Titan's orbital eccentricity (see Eq. 3) and the potential due to Titan's obliquity (see Eq. 4).

The eccentricity potential is given by (Dermott and Sagan 1995)

$$\phi_{ecc} = -\frac{GM_s}{a}\left(\frac{R_T}{a}\right)^2 3e \left(0.5(3\sin^2\theta\cos^2\lambda - 1)\cos(nt) + \sin^2\theta\sin(2\lambda)\sin(nt)\right) \quad (3)$$

where $G = 6.67259 \times 10^{-11}\ \frac{\mathrm{m}^3}{\mathrm{s}^2\mathrm{kg}}$ is the universal gravitational constant, $M_s = 5.685 \times 10^{26}$ kg is Saturn's mass, $a = 1.221865 \times 10^9$ m is the semi-major axis of Titan, $R_T = 2,574,730$ m is Titan's radius, $e = 0.0288$ is Titan's orbital eccentricity, $n = 4.5601 \times 10^{-6}\ \mathrm{s}^{-1}$ is Titan's orbital angular velocity, t is the time measured from perikron (point on Titan's orbit closest to Saturn), θ is the colatitude, and λ is the longitude.

The potential due to the obliquity is (Tyler 2008)

$$\phi_{ob} = \frac{3}{2}n^2 R_T^2 \theta_0 \sin\theta\cos\theta\,(\cos(\lambda - nt) + \cos(\lambda + nt)) \quad (4)$$

where $\theta_0 = 5.34 \times 10^{-3}$ is the obliquity of Titan expressed in radian.

Another forcing which could generate significant surface displacements and currents is the wind. Due to the lack of information about its strength and orientation (see Section 2.1), the influence of wind will partially be discussed (see Section 4.3). The wind forcing is modeled by means of an empirical Earth-based model: the wind-induced surface stress is

$$\boldsymbol{\tau}^s = C_D \rho_{atm} |\boldsymbol{u}_{10}|^2 \frac{\boldsymbol{u}_{10}}{|\boldsymbol{u}_{10}|} \quad (5)$$

with C_D, the drag coefficient; $\rho_{atm} = 5.6\ \mathrm{kg/m}^3$, the atmosphere density; and $\boldsymbol{u}_{10}$, the wind velocity 10 m above ground level (see, e.g., Drews 2013). According to Drews (2013), C_D is about 1.2×10^{-3} on Earth lakes when $u_{10} < 11\ \mathrm{ms}^{-1}$. This condition is encountered by the wind predicted by means of the different GCMs (see Section 2.1)

3.3 Meshing

The shoreline contour, derived from Radar images, is presented on Fig. 3a and the mesh used to implement *bathy A* is shown on Fig. 3b.

The unstructured meshes are generated by means of GMSH (see Geuzaine and Remacle, 2009, http://geuz.org/gmsh/). It is one of the most widely used open source unstructured grid generator and it can generate 2D meshes on a sphere (for further details, see Lambrechts et al. 2008a). We use fully unstructured meshes with a spatial resolution ranging from 1000 to 5000 m. We use three criteria of refinement:

- The local element size is proportional to the celerity of the long surface gravity waves, $c = \sqrt{gh}$, as suggested by Legrand et al. (2006);
- The mesh is refined nearshore to reach a high spatial resolution of 1000 m at the shores (see Fig. 3c);
- The spatial resolution is increased where the bathymetry gradient is the largest and decreases with the distance to this point in order to avoid too many discontinuities between the elements.

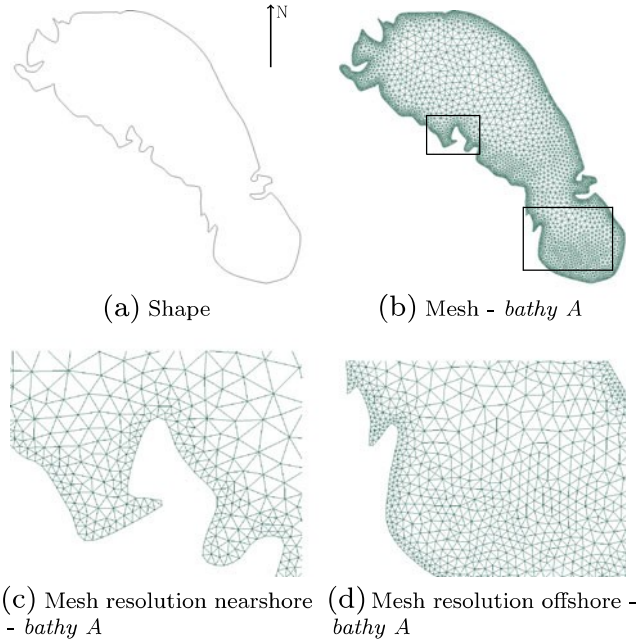

Fig. 3 Discretization of Ontario Lacus using mesh-generation package GMSH: the coastline (**a**) and the mesh used for *bathy A* (**b**). Panel (**c**) shows the higher spatial resolution nearshore. Panel (**d**) shows the refinement in shallow regions in *bathy A*

These meshes allow us to represent as well as possible the coastlines and the bathymetry and to be able to represent the small-scale phenomena occurring nearshore. For *bathy A* and *bathy B*, the local depth is smaller in the south and the spatial resolution is consequently increased in this region. There is no need for increasing the resolution elsewhere; these bathymetries being relatively smooth. The spatial resolution is locally increased offshore for *bathy C* (the spatial resolution offshore remaining larger than 3000 m). As a consequence, the number of triangles varies from one bathymetry to another: it ranges from about 6400 to about 7100.

4 Results

First, a reference simulation, with reference values given in Sections 2.2 and 3.1, is achieved which will allow us to conduct a sensitivity analysis for various bottom frictions, bathymetries and surface stresses. The bathymetry implemented is *bathy C* because it is consistent with the direct depths measured by altimetry from T49 (Mastrogiuseppe at al. 2015 submitted to IEEE) and it is the most recent one.

The sensitivity analysis about bathymetry and bottom friction are respectively conducted in Sections 4.2.1 and 4.2.2.

4.1 Tidal response of Ontario Lacus

The astronomical forcing applied is shown at Fig. 4. It rotates clockwise with an exact period of 1 TD. At any time, the forcing is almost unidirectional over the lake. It has exactly the same magnitude in t^* and $t^* + 0.5$ TD but it is oriented in opposite directions. The maximum magnitude occurs 0.05 TD before perikron/apokron (point on Titan's orbit farthest to Saturn), in the northern part of Ontario Lacus. The predicted local maximum/minimum at 0.25 TD after perikron/apokron are 16 and 13 % weaker than their respective values at perikron/apokron. This forcing is slightly larger than that observed on Earth (due to the Moon and the Sun): a rough approximation gives a maximum value of about 1.7×10^{-6} ms^{-2} at the equator on the closest point of the Moon while the minimum value, in the southern part of Ontario Lacus, is 2.46×10^{-6} ms^{-2}.

The Fourier analysis shows that, except at the amphidromic point of the first tidal component (see Fig. 5b), the first tidal component is responsible for more than 95 % of the amplitude of the lake surface displacements. This is why the other components are not shown. This amphidromic point is located in the center of the lake, at (72.21° S; 175.27° E). At this location, the surface displacements are due to the other tidal components and the sea surface consequently oscillates faster (with a frequency of 1.23×10^{-5} Hz instead of 7.26×10^{-7} Hz).

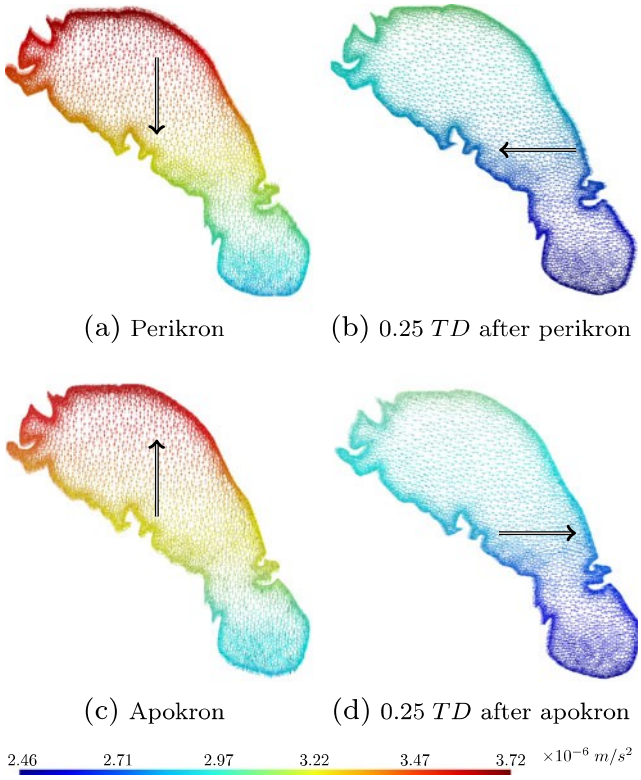

Fig. 4 Instantaneous maps of the acceleration caused by Saturn in Ontario Lacus at four different times (perikron, 0.25 TD after perikron, apokron and 0.25 TD after apokron) (the *black arrows* represent the mean direction). It rotates clockwise with an exact period of 1 TD and it is maximum in the northern part of the lake

Figure 5 shows the tidal range and the tidal phase of the main tidal component over the whole lake. Like the forcing (see Fig. 4), it rotates clockwise (see Figs. 5b and 6). The contribution of the main tidal component to the tidal range is zero at the amphidromic point and increases with the distance to this point. The maximum tidal range (0.563 m) is located in the southern part of the lake (see Fig. 5a). The isolines in Fig. 5a have an ellipsoidal shape, which indicates interactions with the shoreline. The tidal range is higher near the northern and southern shores of Ontario Lacus than near the eastern and western shores (see Figs. 5a and 6), which matches with the evolution of the forcing magnitude and orientation during 1 TD.

Figure 6 shows the instantaneous surface elevation in Ontario Lacus at four orbital phases. The clockwise rotation is noticeable. The maximum and minimum surface elevation will respectively be reached 0.11 TD before the instantaneous map shown in Fig. 6a, c. Such a tidal response could generate dry area(s). With this bathymetry implemented, we do not detect dry areas but it does not mean that there is

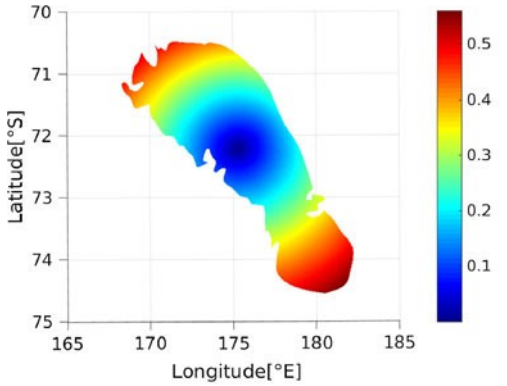

(a) Tidal range of the main component (in meters)

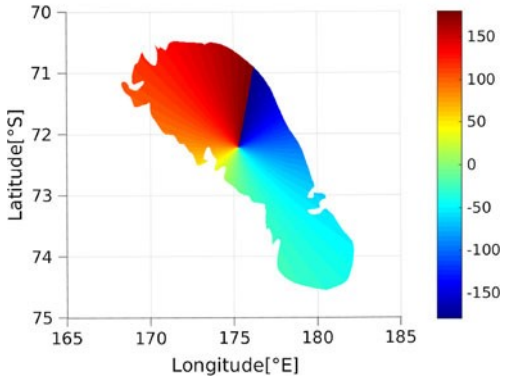

(b) Tidal phase of the main component (in degrees)

Fig. 5 (**a**) Tidal range and (**b**) tidal phase of the main tidal component in Ontario Lacus. The range is the difference between high tide and low tide. The cotidal lines (line of constant tidal phase) merge at the amphidromic point which is located at (72.21° S; 175.27° E). Panel (**b**) shows that the tide rotates clockwise. The tidal range increases with distance to the amphidromic point and is maximum (0.563 m) in the southern part of the lake

no tidal flats in Ontario Lacus. Indeed, such phenomenon could be generated out of the boundaries of this domain. For instance, the high tide floods some areas which are dry regarding to the geoid, but these areas are not included in the boundaries of Ontario Lacus as they are implemented. Given the weak shoreline slopes observed by Hayes et al. (2010) (it ranges from 0.5 to 2.7×10^{-3}), tidal flats are likely to exist.

Figure 7 demonstrated that the tidal currents are less than 0.02 ms^{-1} except for some specific nearshore areas. The current magnitude is larger nearshore and, the larger the distance to the coast, the smaller the magnitude. A high speed is observed at some specific nearshore convex regions like peninsula, cape, or the end of bays (this behavior is particularly visible in Fig. 7a, c). Furthermore, the mean speed is higher when Titan is next to the apokron/perikron: the speed increases over the whole lake and the high-speed areas observed nearshore spread (see Fig. 7). Unlike the astronomical forcing, the tidal current is not always the same in t^* and $t^* + 0,5$ TD and, for $t^* \in [0.325; 0.5]$ TD, the maximum speed is larger in t^* than in $t^*+0.5$ TD. The maximum speed, about 0.037 ms^{-1}, is predicted near area P (see Fig. 1) 0.445 TD after perikron. As the different figures in Fig. 7 show, the maximum current magnitude at a given time is located either in area P (Fig. 7b, d) or in area Q (Fig. 7a, c) but it does not have a constant magnitude over time. Such current acceleration near headlands is also observed on Earth (e.g., in the Irish sea (see Figure 4 in Howarth 2005), in the Baltic sea (see Figure 5.3 in Volkov et al. 2002), in the North sea (see Figure 1.4 in the review from Otto et al. 1990).

The tidal current is globally directed from low to high tide. The current forms one closed loop in which the current magnitude is quite weak in the north (see Fig. 8a, b). There is also a stronger current which goes along Ontario Lacus shores around the lake. These two flow patterns are anticlockwise at perikron and clockwise at apokron. In the narrow part of Ontario Lacus (Area N and R on Fig. 1), the current offshore is a transition between these two patterns while current nearshore is due to liquid exchanges between these two parts. The transition between clockwise and anticlockwise patterns is quick and results in helter-skelter currents.

Rotating shallow water waves such as Kelvin waves and Poincaré waves should not appear in Ontario Lacus. Indeed, the Rossby deformation radius $R = \frac{\sqrt{gh}}{|f|}$ (where the mean depth h is about 27.3 m in this case) is about 700 km which is larger than Ontario Lacus and makes Kelvin waves and long Poincaré waves impossible in this lake. For R larger than the characteristic length scale, the shallow water waves tend to be non dispersive as their phase speed tends to $c \approx \sqrt{gh}$. Such waves are referred to as external gravity waves and are little affected by Titan's rotation. Consequently, surface gravity waves of phase speed $c \approx 6$ ms^{-1} and with a time scale of about 33,000 s (0.02 TD) could appear in Ontario Lacus.

4.2 Influence of bathymetry and bottom friction

First, the results obtained with *bathy A* and *bathy B* are compared to each other and with respect to *bathy C* in terms of tidal current (Figs. 9, 10, 11, and 12) and surface elevation (Fig. 13a, b). Second, the impact of bottom friction is studied by varying Manning's coefficient.

4.2.1 Bathymetry influence

Modifications in the bathymetry have a significant impact on the current (see Figs. 9, 10, 11, and 12) but the main characteristics such as speed decreasing with distance to the shore and acceleration at some specific areas such as headlands are still present.

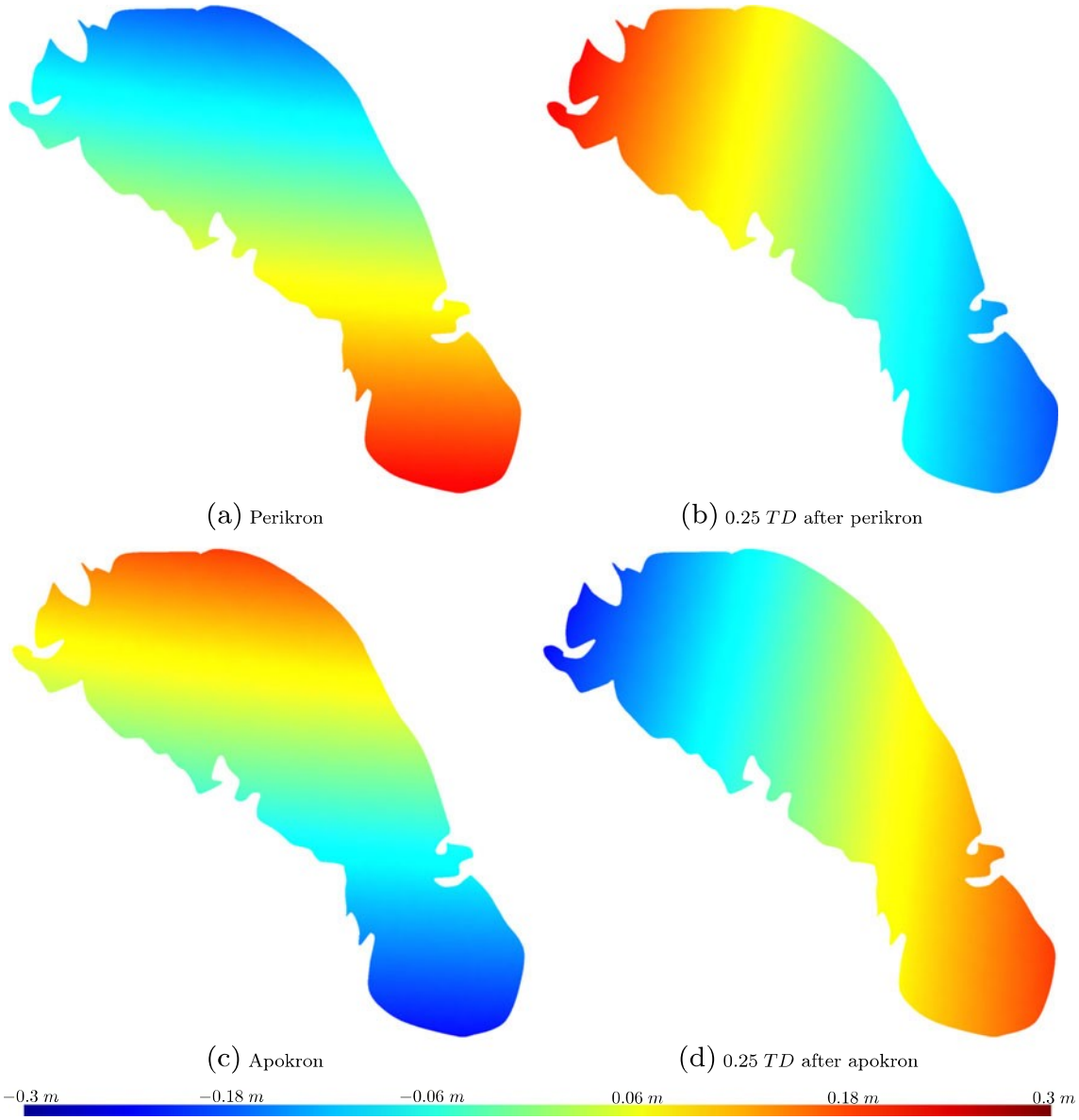

Fig. 6 Surface elevation (in meters) in Ontario Lacus at (**a**) Perikron, (**b**) 0.25 TD after Perikron, (**c**) Apokron, and (**d**) 0.25 TD after Apokron with *bathy C* implemented. The tide is high in the southern part at perikron and rotates clockwise with an exact period of 1 Titan day. The maximum/minimum surface elevation respectively occurs 0.11 TD before perikron/apokron, in the south

With *bathy A* implemented, the current magnitude nearshore is globally smaller (especially at perikron and apokron) but the maximum speed (about 0.046 ms^{-1}) is larger. The maximum speed area is also located nearshore but it is not located near the same peninsula as with *bathy C*. A wide offshore high-speed area is noticeable (especially on Fig. 9b, d): it corresponds with a shallower area (about 3 m depth) separating two deeper areas. In this shallow area, the current is unidirectional along the longitudinal axis of the lake: it is northward at perikron and southward at apokron (see Fig. 10). Due to this area, the closed loop formed by the flow in the north is much smaller. Small circular flow patterns appear during transitions between perikron and apokron but they disappear quickly and correspond to a weak current magnitude.

With *bathy B* implemented, the maximum speed is about 0.032 ms^{-1} and is located near the same headland as with *bathy C*. Similarly to the two other cases, the current magnitude is larger nearshore. Nevertheless, such high-speed areas are not located near the same headlands as with the other bathymetries. For instance, at point R (see Fig. 1), the speed is significantly larger than with *bathy C*, which meets the results obtained with *bathy A*. The northern closed loop has the same shape as with *bathy C* but another closed loop also appeared in the southern part of Ontario Lacus (see Fig. 12a, b). This closed loop and the northern one appear

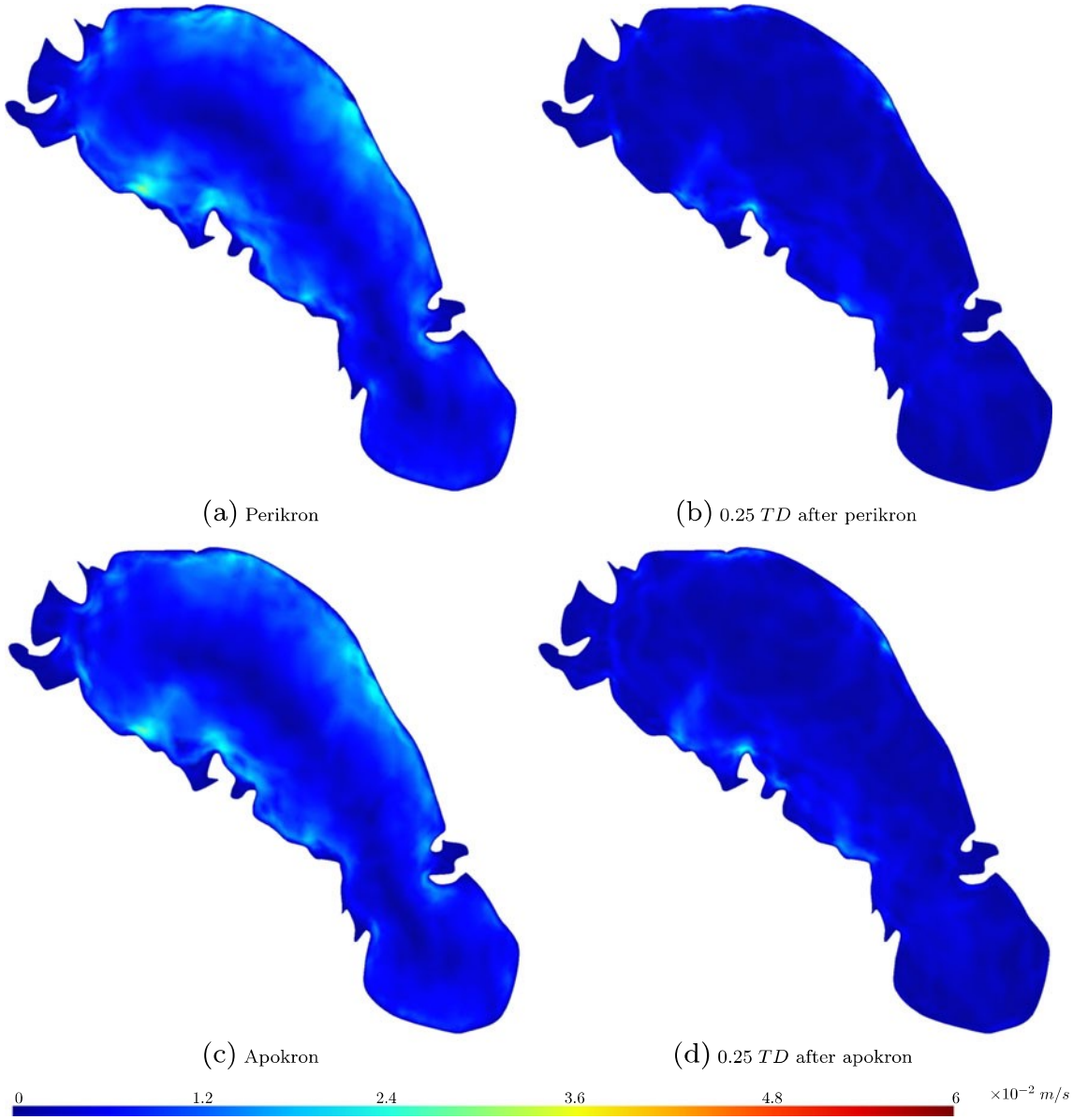

Fig. 7 Tidal current magnitude (in ms^{-1}) in Ontario Lacus at (**a**) perikron, (**b**) 0.25 TD after Perikron, (**c**) Apokron, and (**d**) 0.25 TD after Apokron with *bathy C* implemented. The current magnitude is maximum nearshore, at areas P or Q (see Fig. 1), depending on the time, and decreases with the distance to the shore. Globally, the speed is higher at perikron and apokron than 0.25 TD after perikron and apokron

and disappear together. During the transition between the clockwise and the anticlockwise closed loop, there is a short period during which the flow is almost unidirectional in Ontario Lacus (it is northward after perikron and southward after apokron). These results show that the nearshore bathymetry plays a significant part in the formation of local high-speed areas nearshore and can also modify the offshore flow patterns.

The bathymetry implemented does not have a significant impact on tidal amplitude: the global behavior is the same but modifications in the bathymetry can induce small local changes on the amplitude. The differences in tidal ranges are less than 5 %. However, according to the bathymetry, dry areas can appear and disappear due to the tide (see Fig. 13a, b). They appear while the tide has been low in the southern part or in the northern part of Ontario Lacus. As discussed in Section 4.1, tidal flats could also occur out of the boundaries of this domain, which will increase the size of the areas which can be wet or dry according to the tide.

The size and location of dry areas at low tide vary from one bathymetry to another. With *bathy A*, a dry area appears at the southern end of Ontario Lacus from 0.27 TD (right

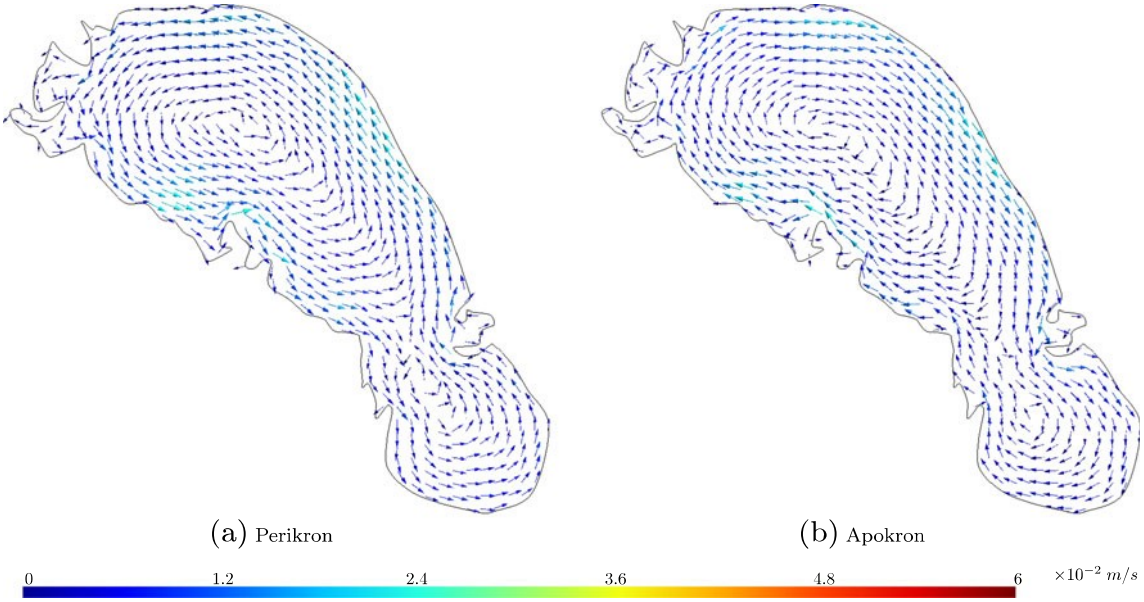

Fig. 8 Tidal current orientation in Ontario Lacus at (**a**) Perikron, and (**b**) Apokron with *bathy C* implemented (the flow is interpolated on a structured grid in order to increase the quality of the figure). The flow forms a closed loop which rotates anticlockwise at perikron and clockwise at apokron

after Fig. 6b) to 0.52 TD (right after Fig. 6c) while, with *bathy B*, there are two of them: a narrow band (at most 1.2 km wide) appearing along the southern coastline and a dry area appearing in a bay at the northern end of Ontario Lacus. The narrow band appears on the south-eastern shore at 0.235 TD (soon before Fig. 6b) and spreads along the shore reaching point N in 0.435 TD. This dry area has totally disappeared by 0.555 TD (soon after Fig. 6c). The second dry area is much smaller: it appears at 0.73 TD and disappears by 0.985 TD. The differences in size and shape of such tidal flats between the bathymetries are due to the variations in terms of local depth (see Fig. 2) and in the bathymetry slope nearshore. For instance, Fig. 2b shows that *bathy B* is shallower in its south-eastern part, which results in a narrow band of dry area along the shore (see Fig. 13b) not observed with other bathymetries.

4.2.2 Bottom friction influence

Common values of Manning's coefficient vary from 0.01 to 0.05 $\mathrm{sm}^{-1/3}$ (which respectively correspond to smooth man-made channel and to natural channels with stones on Earth). The value $\mu = 0.01\ \mathrm{sm}^{-1/3}$ being unlikely on Titan, we studied values from 0.02 to 0.05 by step of 0.01 and an extreme case with a coefficient of $\mu = 0.1\ \mathrm{sm}^{-1/3}$, which corresponds to flooded areas with dense brush on Earth.

Figure 14 shows that, as expected, the flow slows down as Manning's coefficient increases. The high-speed areas along the shore shrink and the speed decreases faster than elsewhere in the lake while bottom friction increases. The maximum speed area over the lake remains nearshore but its location varies with Manning's coefficient. The elevation remains almost constant as μ is modified (not shown): at a given time t^*, the difference is less than 0.3 %.

4.3 Wind orientation influence

In this section, we study the impact of the wind forcing on surface displacements and currents. The wind influence in shallow water equations is represented by the surface stress term $\boldsymbol{\tau}^s$ in Eq. 1 and is modeled by Eq. 5.

Tokano and Lorenz (2015) have already studied wind-driven flows in Titan's sea: they discussed the wind-driven flows in Kraken and Ligeia Mare on a large time scale (1 Titan year) by neglecting the tides. They used the same ocean circulation model as in Tokano et al. (2014). The wind speed and orientation were given by the GCM described in Tokano (2009). They showed that the wind-driven circulation is insignificant except from late spring to late summer in the north. They have also shown that, if the wind is strong, a noticeable veering of the current takes place which is in line with the Ekman spiral theory.

Unlike Tokano and Lorenz (2015), we study wind-driven flows on a short time scale and the tides are taken into account. In this context (see Section 2.1), extreme conditions[11] are implemented: four strong (1 ms^{-1}) unidirectional winds blowing during 1 TD. The impact of such a wind has been studied during the period during which it has

[11] Such a wind speed is strong in comparison with Titan standards: the wind is lower than 0.7 ms^{-1} most of the time.

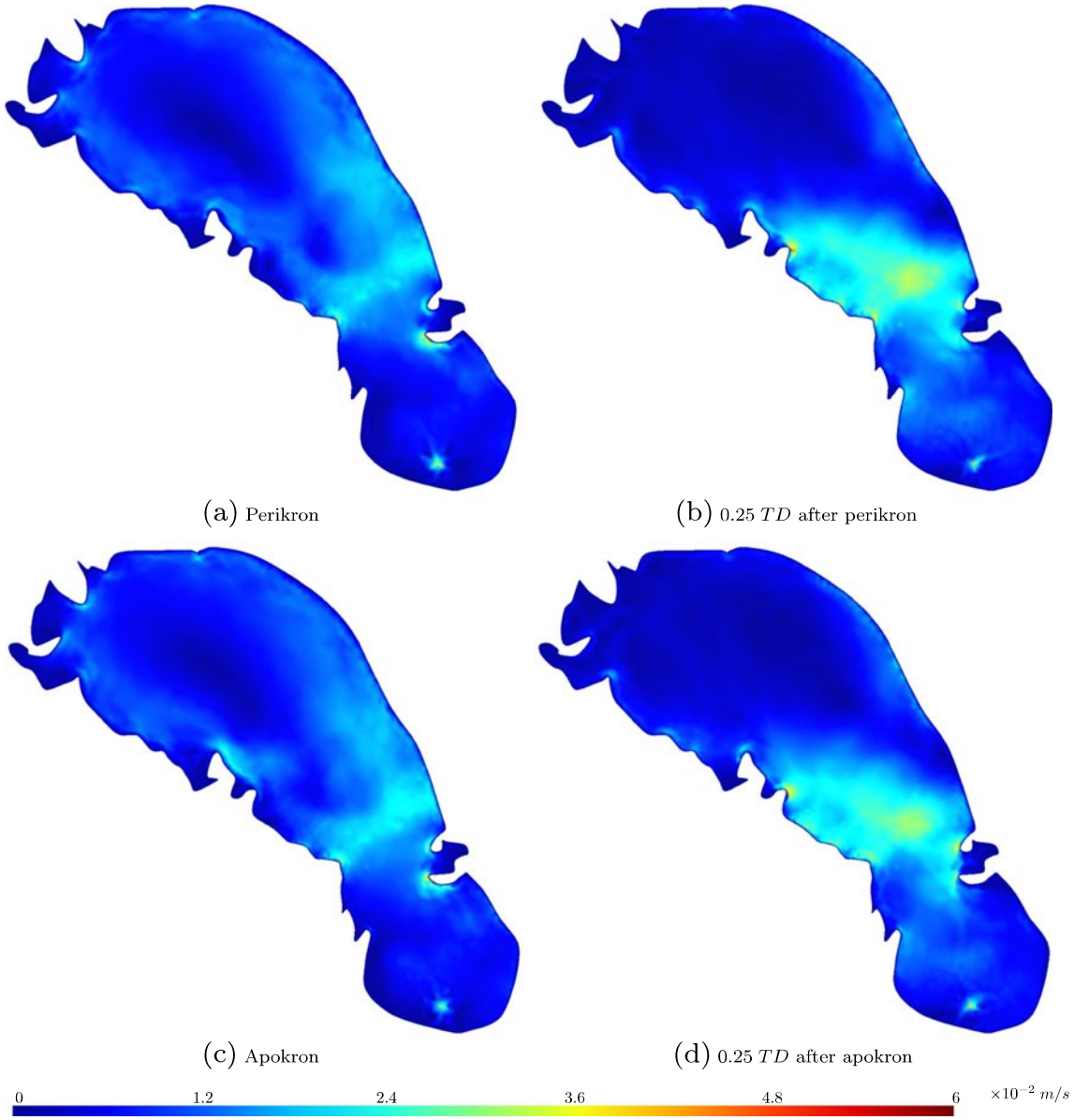

Fig. 9 Tidal current magnitude (in ms^{-1}) in Ontario Lacus with *bathy A* implemented at (**a**) Perikron, (**b**) 0.25 TD after Perikron, (**c**) Apokron, and (**d**) 0.25 TD after Apokron. The current magnitude is maximum nearshore, at area 0 (see Fig. 1) and decreases with the distance to the shore except near area N and R where a wide offshore unidirectional high-speed area is predicted

been blowing and after. Cases 1 to 4, respectively, correspond to southerly, westerly, northerly, and easterly wind. We are aware that such hypothetical winds are unlikely but it allows us, despite the limitations due to the lack of direct observations, to assess how significant the wind forcing is on the regime of Ontario Lacus. Indeed, except at Huygens landing site, there is no in situ measurements of surface wind on Titan. Several studies predicted the wind by means of a GCM (see Section 2.1) but the time scale and the spatial resolution of such simulations are several orders of magnitude larger than those used in our model. In order to overcome this lack of information, a mesoscale model should be used to compute the surface stress but this is beyond the scope of the present study.

The results show that the wind has a significant impact on the flow and on the lake surface elevation. For instance, in case 1, the high tide and the low tide surface elevation of the lake decrease respectively by 0.025 m (∼8.9 %) and 0.044 m (∼15.6 %) where the tidal range of the first tidal component is maximum in the reference case

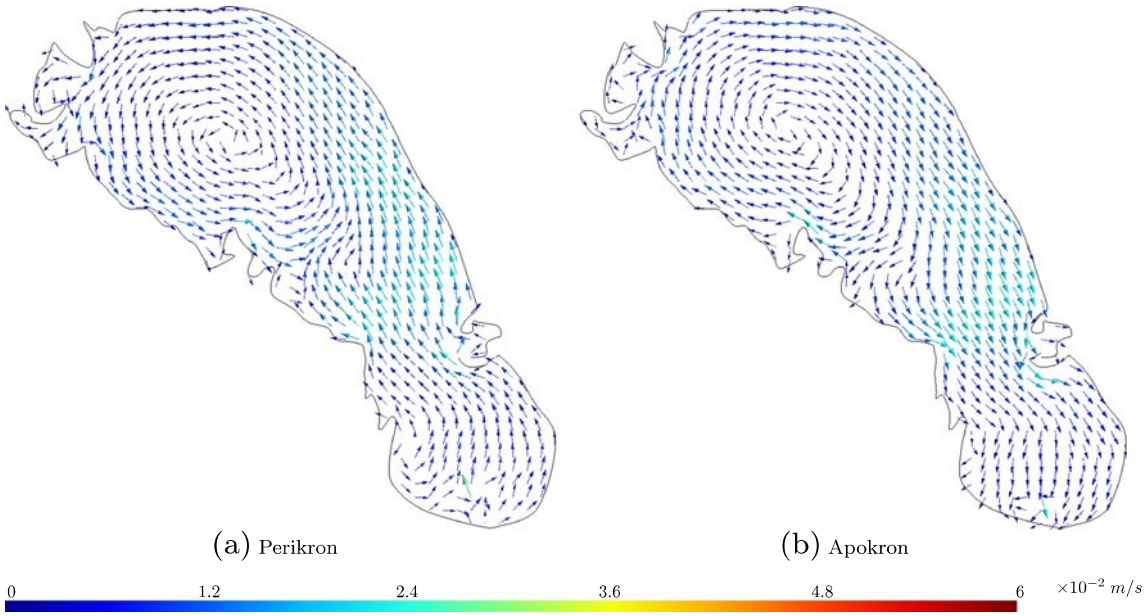

Fig. 10 Tidal current orientation in Ontario Lacus with *bathy A* implemented at (**a**) Perikron and (**b**) Apokron (the flow is interpolated on a structured grid in order to increase the quality of the figure). As with *bathy C*, a closed loop is noticeable in the north. In the offshore high-speed area near point N and R (see Fig. 1), the current is unidirectional along the lake axis (it is northward at perikron and southward at apokron)

(see Section 4.1), which results in a higher range in this region (see Fig. 15) and a lower mean surface elevation, which cannot be neglected. This effect varies with the wind direction.

Due to the wind, the surface elevation does not behave as a pure sinusoid and a constant value has to be added to the tidal components. This wind set-up can represent up to 40 % of the total surface elevation according to the location. For instance, in case 1, this component is maximum in the south: 0.072 m, which represents 19 % of the total lake surface elevation range at this location.

These extreme winds also increase the current magnitude up to more than 390 % according to the location (not shown). New high-speed areas appear near- and off-shore. The current magnitude, the size, and the location of these areas change with the wind orientation. For westerly and easterly wind (cases 2 and 4), the unidirectional high-speed area is oriented along the major axis of the lake and is directed to the left of the surface wind direction (upward for case 2 and downward for case 4) which is an evidence of Ekman transport. This is not observed for northerly and southerly winds, which could be explained by the slender shape of Ontario Lacus. In these cases (cases 1 and 3), there are several unidirectional high-speed areas: one in the north and one in the south of the lake (south of point G, see Fig. 1). They are much smaller and oriented along the wind direction.

The wind influence raises with the time: after 0.06 TD, the northern flow pattern has been strongly modified and after 0.25 TD, it has been replaced by small circular flow patterns around an unidirectional high-speed area which is strongly influenced by the wind direction. In these specific cases, the wind is the main driving force of the current (magnitude and orientation) and has a significant influence on the surface elevation. As soon as the wind stops blowing, its effects slowly decrease. Indeed, after 2 TD, the tidal elevation is maximum at the same location and time than without wind and the difference between the surface elevations is less than 5 % (it is exactly the same after 4 TD). After 5 TD, a closed loop reappears in the flow pattern and, after 7 TD, the pattern is the same as before the wind blew.

A depth-averaged model such as that used in this study suffers from a shortcoming for the simulation of wind-driven flows: the differences between the wind-driven flows near the lake surface and near the lake bottom cannot be simulated. Indeed, the flow will be stronger near the surface and weaker near the lake bottom and the orientation can also differ due to phenomena such as the Ekman spiral. Nevertheless, this model allows us to study the main effects of winds and show that the surface stress due to winds significantly modifies the flow pattern and the tidal amplitude. This is due to the low liquid density (about twice smaller than in Earth's ocean) and the large air density (about 4.5 times larger than at sea level on Earth).

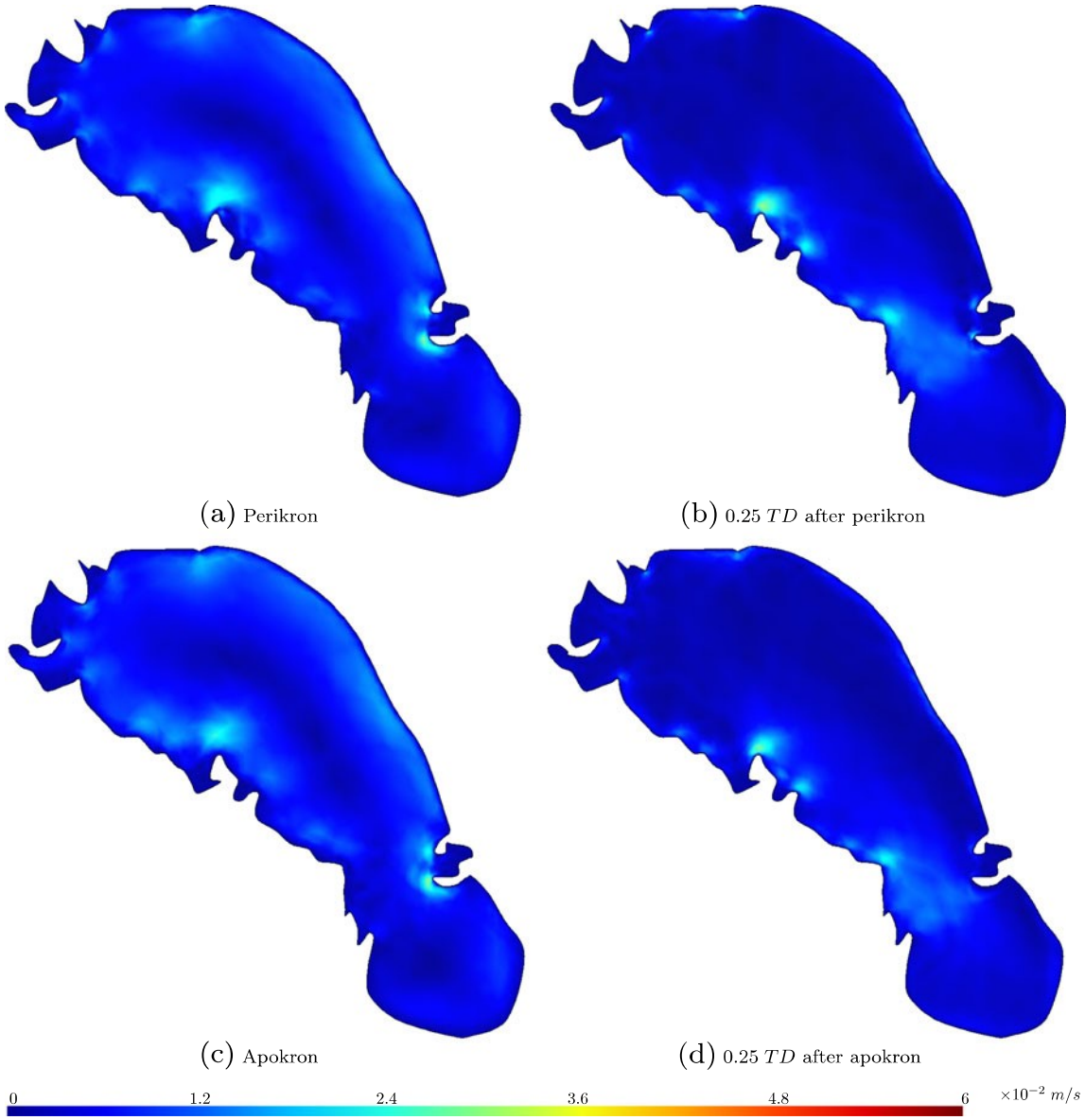

Fig. 11 Tidal current magnitude (in ms^{-1}) in Ontario Lacus with *bathy B* implemented at (**a**) Perikron, (**b**) 0.25 TD after Perikron, (**c**) Apokron, and (**d**) 0.25 TD after Apokron. The current magnitude is maximum nearshore, at area E, and is significantly large at area G

5 Discussion

5.1 Parameter influence

The influence of the molecular diffusivity and the density is studied in the range given by the liquid composition given in the literature (see Section 2.2). Like that of the horizontal diffusivity, the impact of their variation is insignificant (not shown).

The bottom friction tends to decrease the speed all over the lake as it increases. This effect can be more significant in some areas. Moreover, the distribution of high-speed areas also varies with the bottom friction while it does not change the surface elevation.

The bathymetry influence on the velocity is quite different: local circular flow patterns or small acceleration areas can appear over the lake and the maximum speed can vary significantly but the modifications are perceptible on a local scale. The results obtained with the three bathymetries show that the local depth has a significant impact on the velocity, as does the shape of Ontario Lacus: the maximum speed is observed near headlands and the speed is higher nearshore and where the lake is shallow.

Consequently, an accurate shape and bathymetry should be used to properly predict the current magnitude and orientation while we can afford some discrepancy in liquid properties. A particular attention should be paid to the bathymetry as part of a study about the current.

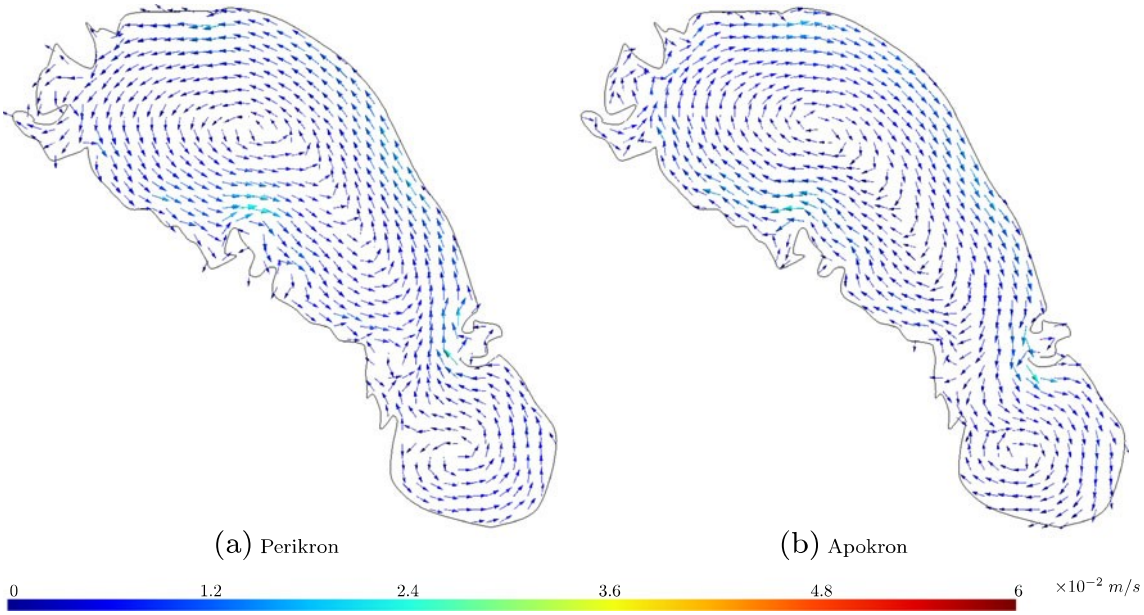

Fig. 12 Tidal current orientation in Ontario Lacus with *bathy B* implemented at (**a**) Perikron and (**b**) Apokron (the current is interpolated on a structured grid in order to increase the quality of the figure). As with the other bathymetries, the flow forms a closed loop in the north. A southern closed loop also appears at perikron and apokron

5.2 Impact of Titan's deformation

The model and the forcings implemented compute the tidal response for a purely rigid body. Nonetheless, Titan has a global subsurface ocean. Due to this ocean, solid tides are much more significant than those on Earth. The surface deformations reduce the tidal forcing exerted by Saturn on the lakes/seas on Titan surface. To take into account such deformation, Sohl et al. (1995), Lorenz et al. (2014), and Tokano et al. (2014) suggested to multiply the

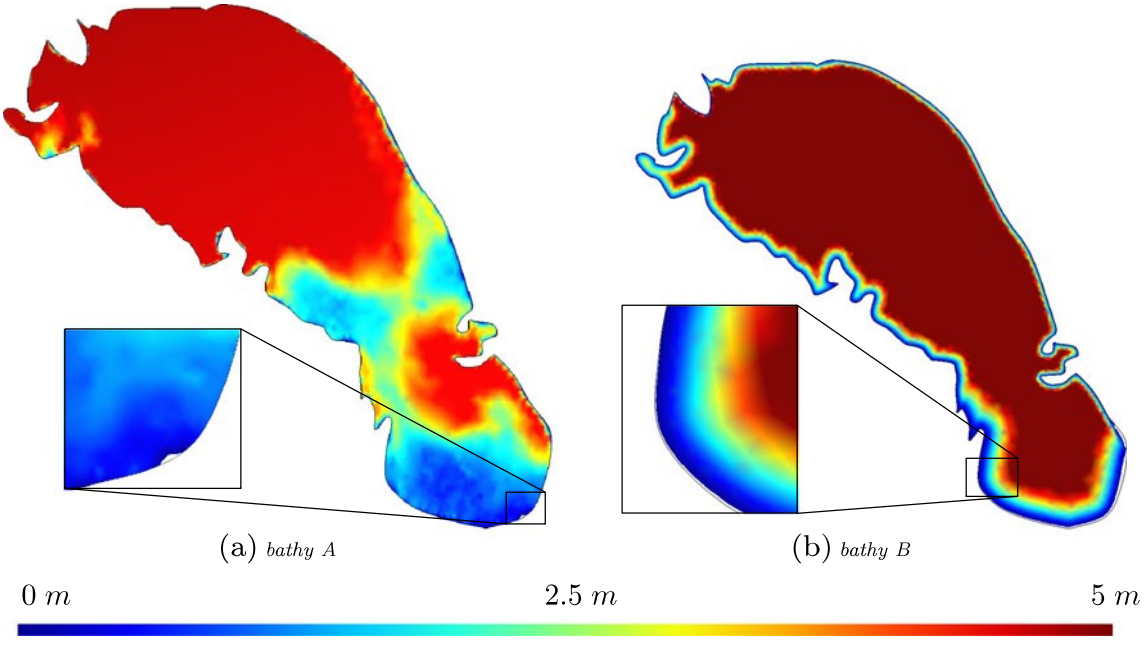

Fig. 13 Map of the total liquid depth (bathymetry + surface elevation) respectively with *bathy A* (**a**) and *bathy B* (**b**) implemented. The depth is cropped at 5 m in order to highlight the dry areas generated by tidal motion and the areas where there is not much liquid remaining. Most of the dry areas are located in the south while shallow areas can also be found offshore and on the eastern shore and on the north-western shore for *bathy A*. With *bathy B* implemented, there are more dry areas and they are larger

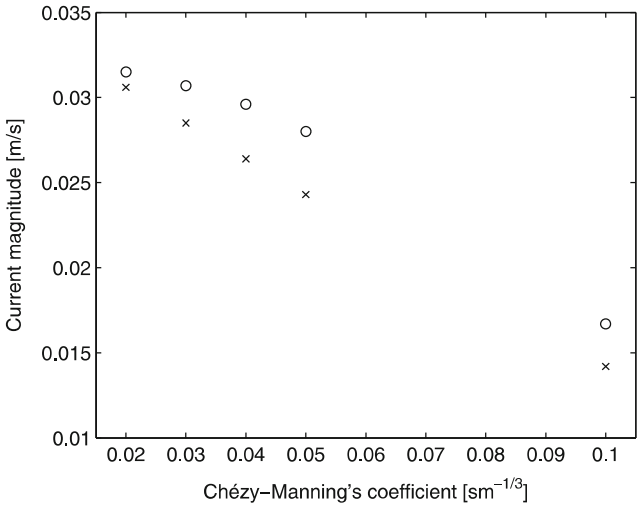

Fig. 14 Evolution of maximum current speed with respect to the Manning's friction coefficient at two different times: perikron (*circle*) and apokron (*cross*). As expected, the flow decreases as the bottom friction increases

forcing by a reduction factor γ_2 function of the degree-2 tidal potential Love number (k_2) and the degree-2 radial displacement Love number (h_2): $\gamma_2 = 1 + \Re(k_2) - \Re(h_2)$. k_2 can be inferred from Cassini measurements (k_2 ranges from 0.589 ± 0.075 to 0.637 ± 0.112) (Iess et al. 2012) but there are uncertainties about h_2 which is predicted by models assuming ice shell and interiors properties which are not well known (for instance, h_2 varies linearly with the ice shell thickness Sohl et al. (2003)). Considering plausible h_2 values, γ_2 is expected to vary between 0 and 0.21 (Tokano et al. 2014; Beuthe 2015). Considering the uncertainties in γ_2, we decided to present the results for a rigid Titan keeping in mind that it provides an upper bound of the tidal range.

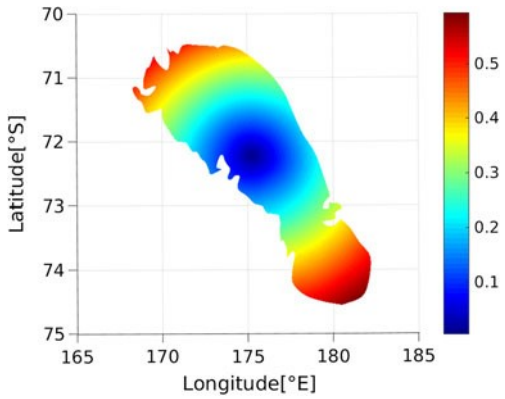

Fig. 15 Lake surface elevation range in Ontario Lacus with a southerly wind of 1 ms^{-1} blowind during 1 TD. It is higher in the south (due to the higher contribution of the constant term): the maximum lake surface elevation range is 0.593 m

5.3 Shoreline variations

Although the shoreline variations due to the tides are difficult for Cassini to observe, it remains an interesting question. According to the bathymetry implemented, the size and the location of dry areas appearing at low tide vary. The largest are obtained with *bathy B*: with this bathymetry implemented, the dry areas spread out to 1.2 km away from the south-western shore at low tide while the largest dry area predicted with *bathy A* implemented spreads out to 0.8 km away from the southern shore (see Fig. 13b). These variations are those due to the low tide. By adding the dry areas which are flooded at high tide, one gets a variations of, respectively, 2.4 and 1.6 km. At point N (see Fig. 1), the tidal range predicted by means of our model is at most 0.35 m. Assuming the smaller slope from Hayes et al. (2011) (1.1×10^{-4}), it would result in 3.2 km length of land that could be submerged depending on the tide. Such variations are significant and could be observed by Cassini but they remains smaller than the observed recession (which are respectively ~10 km in the southwest corner and about 20 km at point N (Turtle et al. 2011; Hayes et al. 2011)). These values are an upper bound: in order to observe such variations, the time lag would have to be exactly 0.5 TD. Moreover, as discussed previously, the solid tides attenuate the tidal range. Consequently, tidally induced shoreline variations are very unlikely to be observed by Cassini.

In the light of the time lag between the 2005 ISS images and the 2009 SAR observations (94.67 TD) and between the 2005 and 2009 ISS images (87.17 TD), the difference in surface elevation is lower than the predicted tidal range and, although significant, the predicted tidal flats are much smaller than the observed shoreline variations. The wind could increase the size of the tidal flats (for instance, with the extreme northerly wind previously studied, the maximum lake surface elevation range in the south is 0.592 m, which results in a tidal flat of 5.39 km wide) but not enough to generate a 20 km length variation. Moreover, it would not explain the recession observed on both eastern and western shores. As a consequence, either other phenomena such as evaporation play a significant part in the shoreline recession (2005 ISS observations were made close to the mid southern summer while 2009 ISS and SAR observations are close to the vernal equinox) or the variations are due to the low spatial resolution of ISS observations in 2005.

5.4 Intercomparison with previous results and Lake Ontario

Numerical simulations of Ontario Lacus tidal response have already been performed by Tokano (2010). Our predictions have some similarities but there also are significant differ-

ences. In both simulations, the tidal amplitude is maximum in the southern part of the lake and the surface elevation is larger at apokron and perikron than 0.25 TD later. Nevertheless, our model predicts a maximum tidal range which is about three times larger than that predicted by Tokano (2010) (about 0.563 m instead of 0.2 m) while Barnes et al. (2009) and Hayes et al. (2011), using analytical approaches, both predicted a maximum tidal range of 0.4 m in the southern part of the lake. Furthermore, Tokano (2010) predicted a purely longitudinal motion along Ontario Lacus longitudinal axis while, according to our results, the tide rotates clockwise with an exact period of 1 TD, which is consistent with the forcing. The current magnitude and orientation is also quite different: Tokano (2010) predicted a purely longitudinal current (along the longitudinal axis of the lake) with a maximum speed of about 0.003 ms^{-1} located offshore while the flow predicted by our model forms closed loop(s), the maximum speed is located nearshore and can locally reach up to 0.046 ms^{-1}, and a mean speed of about 0.02 ms^{-1} is predicted. This could be partially explained by the constant depth and the simplified shape used by Tokano. Indeed, the shallow area and the headlands have a significant influence on the current.

For a better comparison, a 20 m constant depth, a larger spatial resolution of 10 km, and a quadratic bottom friction law have also been implemented in order to be as close as possible to Tokano's simulations (not shown). Nevertheless, it remains an unstructured grid made of triangles while Tokano used a structured grid with equidistant grid points and the shape of the domain is simpler in Tokano (2010). Our simulation shows that the tidal range remains close to 0.56 m and the current is not unidirectional, which is consistent with the rotational tides predicted with a realistic bathymetry. The speed is smaller than 0.02 ms^{-1} which is closer to Tokano's prediction.

Lake Ontario, the terrestrial counterpart, is slightly larger (311 km × 85 km) and deeper (the mean depth is 86 m). It is located at a lower latitude and its longitudinal axis is almost perpendicular to the longitude axis. In Lake Ontario, the tidal range caused by the Moon and the Sun is less than 5 cm (National Oceanic and Atmospheric Administration 2014), which is one order of magnitude smaller than that predicted by means of our model for Ontario Lacus, but it increases significantly due to wind and barometric pressure changes (Hamblin 1982; National Oceanic and Atmospheric Administration 2014). If we multiply the predicted tidal range in Ontario Lacus by a reduction factor of $\gamma_2 = 0.1$ (it is the value used by Tokano et al. (2014)) as done by Lorenz et al. (2014), we would obtain a tidal range which is in the same order of magnitude as the one observed in Lake Ontario. The difference in the tidal range could also be explained by the fact that the gravity on Titan and the Coriolis factor are smaller while the tidal potential is larger than that on Earth.

Hamblin (1982) computed the tide in Lake Ontario by taking into account the forcing due to the moon, the sun and the wind, and compared its results with in situ measurements. He took into account the first four modes with a period of, respectively, 5.06, 3.21, 2.32, and 1.705 h. The periods are quite different from those observed in Ontario Lacus, which is due to the forcing: the orbital period of Titan around Saturn is much larger and we did not take into account the forcing due to the wind, the Sun, and the other moons. He observed and predicted that the phase of the main mode progresses in a anticlockwise sense, which is the opposite of our results in Ontario Lacus. This is due to the fact that Lake Ontario is in the northern hemisphere and Ontario Lacus is located in the southern hemisphere.

6 Conclusion

Titan is, with Earth, the only celestial body of the solar system presenting large liquid bodies on its surface. In this paper, we have studied Ontario Lacus, the largest lake in Titan southern hemisphere. SLIM (www.climate.be/slim), a model solving the 2D depth-averaged shallow water equations by means of the discontinuous Galerkin finite element method, was adapted to Titan conditions (e.g., gravitational acceleration, tidal forcing) in order to simulate the tidal response of this lake. The influence of bathymetry and bottom friction was studied through three different bathymetries and various Manning's coefficient values. The influence of wind has also been roughly assessed.

Our model predicts a clockwise rotating tide with an exact period of 1 TD. The maximum tidal range (about 0.56 m) occurs in the southern part of the lake. At perikron, the tide is high in the south. The current magnitude varies over the lake: it is maximum nearshore and decreases with the distance to the shore. The maximum is located next to headland(s), on the western shore. Its magnitude and location vary with the bathymetry implemented. According to the bathymetry, it can reach up to 0.046 ms^{-1} while the speed offshore is about 0.02 ms^{-1}. The current magnitude is also higher where the lake is shallower. The flow forms a closed loop in the northern part. Despite many differences (e.g., gravitational acceleration, Coriolis factor, location, liquid properties, astronomical, and wind forcing), our results exhibit similarities with the tide observed in Lake Ontario.

We studied the tidal response for the three bathymetries derived from Cassini data. The wind and the bottom friction were also discussed. The bathymetry and the bottom friction can significantly modify the current. Indeed, bathymetry variations induce some changes in current patterns and some local high-speed areas can appear or disappear. This effect is particularly significant in shallow regions. The bottom

friction has a global effect: while it increases, the current speed decreases. Bathymetry and bottom friction both have a very small impact on elevation, although the bathymetry can significantly modify the appearance of dry areas of various shapes and sizes.

We studied four hypothetical winds which would be considered as weak reported to the terrestrial standards but are among the strongest predicted by means of GCMs on Titan. Such unidirectional and strong winds are highly unlikely on Titan but their influence on the flow can be significant. Their impact strengthens with time when they are unidirectional and, in these particular cases, their effect continued to be felt after it died during 4 TD for the elevation, and during 7 TD for the current.

In the future, this model could be used to predict the tidal response of the sea where a capsule could land such as Ligeia Mare for the TIME (Titan Mare Explorer) capsule (Lorenz et al. 2012).

Acknowledgments The present study was carried out in the framework of the project "Taking up the challenge of multiscale marine modelling," which is funded by the Communauté Française de Belgique under contract ARC 10/15-028 with the aim of developing and using SLIM (www.climate.be/slim). David VINCENT is a PhD student funded by a grant of the Fonds spéciaux de recherche of the Université catholique de Louvain, Eric DELEERSNIJDER is an honory research associate with the Belgian Fund for Scientific Research (FNRS), Özgür KARATEKIN is funded by the belgian PRODEX, managed by the ESA, in collaboration with th Belgian Federal Science Policy Office.

We would like to thank N. GUILLAUME for his previous work as a Master's degree student at Université catholique de Louvain and the SLIM team for their support.

References

Aharonson O, Hayes AG, Lunine JI, Lorenz RD, Allison MD, Elachi C (2009) An asymmetric distribution of lakes on Titan as a possible consequence of orbital forcing. Nat Geosci 2(12):851–854. doi:10.1038/ngeo698

Barnes JW, Brown RH, Soderblom JM, Soderblom LA, Jaumann R, Jackson B, Le Mouélic S, Sotin C, Buratti BJ, Pitman KM et al (2009) Shoreline features of Titan's Ontario Lacus from Cassini/VIMS observations. Icarus 201(1):217–225. doi:10.1016/j.icarus.2008.12.028

Bernard PE, Chevaugeon N, Legat V, Deleersnijder E, Remacle JF (2007) High-order h-adaptive discontinuous galerkin methods for ocean modelling. Ocean Dyn 57(2):109–121. doi:10.1007/s10236-006-0093-y

Beuthe M (2015) Tidal Love numbers of membrane worlds: europa, Titan, and Co. Icarus 258(57):239–266. doi:10.1016/j.icarus.2015.06.008

Brown RH, Baines KH, Bellucci G, Bibring JP, Buratti BJ, Capaccioni F, Cerroni P, Clark RN, Coradini A, Cruikshank DP et al (2004) The Cassini visual and infrared mapping spectrometer (VIMS) investigation. In: The Cassini-Huygens Mission. Springer, pp 111–168. doi:10.1007/1-4020-3874-7_3

Brown RH, Soderblom LA, Soderblom JM, Clark RN, Jaumann R, Barnes JW, Sotin C, Buratti B, Baines KH, Nicholson PD (2008) The identification of liquid ethane in Titan's Ontario Lacus. Nature 454(7204):607–610. doi:10.1038/nature07100

De Brye B, De Brauwere A, Gourgue O, Kärnä T, Lambrechts J, Comblen R, Deleersnijder E (2010) A finite-element, multi-scale model of the Scheldt tributaries, river, estuary and ROFI. Coast Eng 57(9):850–863. doi:10.1016/j.coastaleng.2010.04.001

De Brye B, Schellen S, Sassi M, Vermeulen B, Kärnä T, Deleersnijder E, Hoitink T (2011) Preliminary results of a finite-element, multi-scale model of the Mahakam Delta (Indonesia). Ocean Dyn 61(8):1107–1120. doi:10.1007/s10236-011-0410-y

Cordier D, Mousis O, Lunine JI, Lavvas P, Vuitton V (2009) An estimate of the chemical composition of Titan's lakes. Astrophys J Lett 707(2):L128. doi:10.1088/0004-637X/707/2/L128

Cordier D, Mousis O, Lunine JI, Lebonnois S, Rannou P, Lavvas P, Lobo LQ, Ferreira AGM (2012) Titan's lakes chemical composition: sources of uncertainties and variability. Planet Space Sci 61(1):99–107. doi:10.1016/j.pss.2011.05.009

Cottini V, Nixon CA, Jennings DE, de Kok R, Teanby NA, Irwin PGJ, Flasar FM (2012) Spatial and temporal variations in Titan's surface temperatures from Cassini CIRS observations. Planet Space Sci 60(1):62–71. doi:10.1016/j.pss.2011.03.015

Dermott SF, Sagan C (1995) Tidal effects of disconnected hydrocarbon seas on Titan. Nature 374(6519):238–240. doi:10.1038/374238a0

Drews C (2013) Using wind setdown and storm surge on Lake Erie to calibrate the air-sea drag coefficient. PloS ONE 8(8):e72,510. doi:10.1371/journal.pone.0072510

Elachi C, Allison MD, Borgarelli L, Encrenaz P, Im E, Janssen MA, Johnson WTK, Kirk RL, Lorenz RD, Lunine JI et al (2004) Radar: the Cassini titan radar mapper. Space Sci Rev 115(1-4):71–110. doi:10.1007/s11214-004-1438-9

Flasar FM, Kunde VG, Abbas MM, Achterberg RK, Ade P, Barucci A, Bézard B, Bjoraker GL, Brasunas JC, Calcutt S et al (2004) Exploring the saturn system in the thermal infrared: The composite infrared spectrometer. In: The Cassini-Huygens Mission. Springer, pp 169–297. doi:10.1007/1-4020-3874-7_4

Friedson AJ, West RA, Wilson EH, Oyafuso F, Orton GS (2009) A global climate model of Titan's atmosphere and surface. Planet Space Sci 57(14):1931–1949. doi:10.1016/j.pss.2009.05.006

Fulchignoni M, Ferri F, Angrilli F, Ball AJ, Bar-Nun A, Barucci MA, Bettanini C, Bianchini G, Borucki W, Colombatti G et al (2005) In situ measurements of the physical characteristics of Titan's environment. Nature 438(7069):785–791. doi:10.1038/nature04314

Geuzaine C, Remacle JF (2009) Gmsh: a 3-d finite element mesh generator with built-in pre-and post-processing facilities. Int J Numer Methods Eng 79(11):1309–1331. doi:10.1002/nme.2579

Glein CR, Shock EL (2013) A geochemical model of non-ideal solutions in the methane-ethane-propane-nitrogen-acetylene system on Titan. Geochim Cosmochim Ac 115:217–240. doi:10.1016/j.gca.2013.03.030

Hamblin PF (1982) On the free surface oscillations of Lake Ontario. Limnol Oceanogr 27(6):1039–1049. doi:10.4319/lo.1982.27.6.1039

Hanel R, Conrath B, Flasar FM, Kunde V, Maguire W, Pearl J, Pirraglia J, Samuelson R, Herath L, Allison M, Cruikshank D, Gautier D, Gierasch P, Horn L, Koppany R, Ponnamperuma C (1981) Infrared observations of the saturnian system from Voyager-1. Science 212:192–200. doi:10.1126/science.212.4491.192

Hayes AG (2016) The lakes and seas of Titan. Ann Rev Earth Planet Sci:44. doi:10.1146/annurev-earth-060115-012247

Hayes AG, Aharonson O, Callahan P, Elachi C, Gim Y, Kirk RL, Lewis K, Lopes R, Lorenz RD, Lunine JI et al (2008) Hydrocarbon lakes on Titan: distribution and interaction with a porous regolith. Geophys Res Lett 35(9). doi:10.1029/2008GL033409

Hayes AG, Wolf AS, Aharonson O, Zebker H, Lorenz RD, Kirk RL, Paillou P, Lunine JI, Wye L, Callahan P et al (2010) Bathymetry and absorptivity of Titan's Ontario Lacus. J Geophys Res-Planet 115(E9):E09, 009. doi:10.1029/2009JE003557

Hayes AG, Aharonson O, Lunine JI, Kirk RL, Zebker HA, Wye LC, Lorenz RD, Turtle EP, Paillou P, Mitri G et al (2011) Transient surface liquid in Titan's polar regions from Cassini. Icarus 211(1):655–671. doi:10.1016/j.icarus.2010.08.017

Hayes AG, Michaelides RJ, Turtle EP, Barnes JW, Soderblom JM, Masrtogiuseppe M, Lorenz RD, Kirk RL, Lunine JI (2014) The distribution and volume of Titan's hydrocarbon lakes and seas. In: Lunar and planetary institute science conference abstracts, vol 45, p 2341

Howarth MJ (2005) Hydrography of the Irish sea Sea6 technical report. Department of Trade and Industry offshore energy Strategic Assessment programme, UK

Iess L, Jacobson RA, Ducci M, Stevenson DJ, Lunine JI, Armstrong JW, Asmar SW, Racioppa P, Rappaport NJ, Tortora P (2012) The tides of Titan. Science 337(6093):457–459. doi:10.1126/science.1219631

Jennings DE, Flasar FM, Kunde VG, Samuelson RE, Pearl JC, Nixon CA, Carlson RC, Mamoutkine AA, Brasunas JC, Guandique E et al (2009) Titan's surface brightness temperatures. Astrophys J Lett 691(2):L103. doi:10.1088/0004-637X/691/2/L103

Jennings DE, Cottini V, Nixon CA, Flasar FM, Kunde VG, Samuelson RE, Romani PN, Hesman BE, Carlson RC, Gorius NJP et al (2011) Seasonal changes in Titan's surface temperatures. Astrophys J Lett 737(1):L15. doi:10.1088/2041-8205/737/1/L15

Kärnä T, De Brye B, Gourgue O, Lambrechts J, Comblen R, Legat V, Deleersnijder E (2011) A fully implicit wetting-drying method for DG-FEM shallow water models, with an application to the Scheldt Estuary. Comput Method Appl M 200(5):509–524. doi:10.1016/j.cma.2010.07.001

Lambrechts J, Comblen R, Legat V, Geuzaine C, Remacle JF (2008a) Multiscale mesh generation on the sphere. Ocean Dyn 58(5-6):461–473. doi:10.1007/s10236-008-0148-3

Lambrechts J, Hanert E, Deleersnijder E, Bernard PE, Legat V, Remacle JF, Wolanski E (2008b) A multi-scale model of the hydrodynamics of the whole Great Barrier Reef. Estuar Coast Shelf S 79(1):143–151. doi:10.1016/j.ecss.2008.03.016

Lebonnois S, Burgalat J, Rannou P, Charnay B (2012) Titan global climate model: a new 3-dimensional version of the IPSL Titan GCM. Icarus 218(1):707–722. doi:10.1016/j.icarus.2011.11.032

Legrand S, Deleersnijder E, Hanert E, Legat V, Wolanski E (2006) High-resolution, unstructured meshes for hydrodynamic models of the great barrier reef, Australia. Estuar, Coastal Shelf Sci 68(1):36–46. doi:10.1016/j.ecss.2005.08.017

Cornet T, Bourgeois O, Le Mouélic S, Rodriguez S, Lopez Gonzalez T, Sotin C, Tobie G, Fleurant C, Barnes JW, Brown RH et al (2012) Geomorphological significance of Ontario Lacus on Titan: integrated interpretation of Cassini VIMS ISS and RADAR data and comparison with the Etosha Pan (Namibia). Icarus 218(2):788–806. doi:10.1016/j.icarus.2012.01.013

Lorenz RD, Lunine JL, Neish CD (2011) Cyanide soap? Dissolved materials in Titan's seas. EPSC-DPS2011 6:488

Lorenz RD (2013) Oceanography on Saturn's moon, Titan. In: Oceans-san diego, 2013. IEEE, pp 1–7

Lorenz RD, Newman C, Lunine JI (2010) Threshold of wave generation on Titan's lakes and seas: effect of viscosity and implications for Cassini observations. Icarus 207(2):932–937. doi:10.1016/j.icarus.2009.12.004

Lorenz RD, Tokano T, Newman CE (2012) Winds and tides of Ligeia Mare, with application to the drift of the proposed TiME (Titan Mare Explorer) capsule. Planet Space Sci 60(1):72–85. doi:10.1016/j.pss.2010.12.009

Lorenz RD, Kirk RL, Hayes AG, Cassini AG, Anderson YZ, Lunine JI, Tokano T, Turtle EP, Malaska MJ, Soderblom JM, Lucas A, et al (2014) A radar map of Titan seas: Tidal dissipation and ocean mixing through the throat of Kraken. Icarus 237:9–15. doi:10.1016/j.icarus.2014.04.005

Lunine JI, Hayes A, Aharonson O, Mitri G, Lorenz R, Stofan E, Wall S, Elachi C, Cassini Radar Team et al (2009) Evidence for liquid in Ontario Lacus (Titan) from Cassini-observed changes. In: AAS/Division for planetary sciences meeting abstracts# 41, vol 41

Luspay-Kuti A, Chevrier VF, Cordier D, Rivera-Valentin EG, Singh S, Wagner A, Wasiak FC (2015) Experimental constraints on the composition and dynamics of Titan's polar lakes. Earth Planet Sc Lett 410:75–83. doi:10.1016/j.epsl.2014.11.023

Mastrogiuseppe M, Poggiali V, Hayes A, Lorenz R, Lunine J, Picardi G, Seu R, Flamini E, Mitri G, Notarnicola C et al (2014) The bathymetry of a Titan sea. Geophys Res Lett 41(5):1432–1437. doi:10.1002/2013GL058618

McEwen A, Turtle E, Perry J, Dawson D, Fussner S, Collins G, Porco C, Johnson T, Soderblom L (2005) Mapping and monitoring the surface of Titan Bulletin of the american astronomical society, vol 37, p 739

Mitchell KL, Barmatz MB, Jamieson CS, Lorenz RD, Lunine JI (2015) Laboratory measurements of cryogenic liquid alkane microwave absorptivity and implications for the composition of ligeia mare, Titan. Geophys Res Lett 42(5):1340–1345. doi:10.1002/2014GL059475

National Oceanic and Atmospheric Administration (2014) Do the Great Lakes have tides. http://oceanservice.noaa.gov/facts/gltides.html, accessed: 2015-08-21

Niemann HB, Atreya SK, Bauer SJ, Carignan GR, Demick JE, Frost RL, Gautier D, Haberman JA, Harpold DN, Hunten DM et al (2005) The abundances of constituents of Titan's atmosphere from the GCMS instrument on the Huygens probe. Nature 438(7069):779–784. doi:10.1038/nature04122

Otto L, Zimmerman JTF, Furnes GK, Mork M, Saetre R, Becker G (1990) Review of the physical oceanography of the North Sea. Neth J Sea Res 26(2):161–238. doi:10.1016/0077-7579(90)90091-T

Porco CC, West RA, Squyres S, Mcewen A, Thomas P, Murray CD, Delgenio A, Ingersoll AP, Johnson TV, Neukum G et al (2004) Cassini imaging science: instrument characteristics and anticipated scientific investigations at Saturn. Space Sci Rev 115(1-4):363–497. doi:10.1007/s11214-004-1456-7

Sagan C, Dermott SF (1982) The tide in the seas of Titan. Nature 300(5894):731–733. doi:10.1038/300731a0

Samuelson RE, Hanel RA, Kunde VG, Maguire WC (1981) Mean molecular weight and hydrogen abundance of Titan's atmosphere. Nature 292:688–693

Schneider T, Graves SDB, Schaller EL, Brown ME (2012) Polar methane accumulation and rainstorms on Titan from simulations of the methane cycle. Nature 481(7379):58–61. doi:10.1038/nature10666

Sears WD (1995) Tidal dissipation in oceans on Titan. Icarus 113(1):39–56. doi:10.1006/icar.1995.1004

Seny B, Lambrechts J, Comblen R, Legat V, Remacle JF (2013) Multirate time stepping for accelerating explicit discontinuous Galerkin computations with application to geophysical flows. Int J Numer Meth Fl 71(1):41–64. doi:10.1002/fld.3646

Smagorinsky J (1963) General circulation experiments with the primitive equations: I. the basic experiment. Mon Weather Rev 91(3):99–164. doi:10.1175/1520-0493(1963)091<0099:GCEWTP>2.3.CO;2

Sohl F, Sears WD, Lorenz RD (1995) Tidal dissipation on Titan. Icarus 115(2):278–294

Sohl F, Hussmann H, Schwentker B, Spohn T, Lorenz RD (2003) Interior structure models and tidal Love numbers of Titan. J Geophys Res-Planet 108(E12). doi:10.1029/2003JE002044

Stofan ER, Elachi C, Lunine JI, Lorenz RD, Stiles B, Mitchell KL, Ostro S, Soderblom L, Wood C, Zebker H et al (2007) The lakes of Titan. Nature 445(7123):61–64. doi:10.1038/nature05438

Tan SP, Kargel JS, Marion GM (2013) Titan's atmosphere and surface liquid: new calculation using statistical associating fluid theory. Icarus 222(1):53–72. doi:10.1016/j.icarus.2012.10.032

Tan SP, Kargel JS, Jennings DE, Mastrogiuseppe M, Adidharma H, Marion GM (2015) Titan's liquids: exotic behavior and its implications on global fluid circulation. Icarus 250:64–75. doi:10.1016/j.icarus.2014.11.029

Tokano T (2008) Dune-forming winds on Titan and the influence of topography. Icarus 194(1):243–262. doi:10.1016/j.icarus.2007.10.007

Tokano T (2009) Impact of seas/lakes on polar meteorology of Titan: simulation by a coupled GCM-sea model. Icarus 204(2):619–636. doi:10.1016/j.icarus.2009.07.032

Tokano T (2010) Simulation of tides in hydrocarbon lakes on Saturn's moon Titan. Ocean Dyn 60(4):803–817. doi:10.1007/s10236-010-0285-3

Tokano T, Lorenz RD (2015) Wind-driven circulation in Titan's seas. J Geophys Res-Planet 120(1):20–33. doi:10.1002/2014JE004751

Tokano T, Lorenz RD, Van Hoolst T (2014) Numerical simulation of tides and oceanic angular momentum of Titan's hydrocarbon seas. Icarus 242:188–201. doi:10.1016/j.icarus.2014.08.021

Turtle EP, Perry JE, Hayes AG, McEwen AS (2011) Shoreline retreat at Titan's Ontario Lacus and Arrakis Planitia from Cassini imaging science subsystem observations. Icarus 212(2):957–959. doi:10.1016/j.icarus.2011.02.005

Tyler RH (2008) Strong ocean tidal flow and heating on moons of the outer planets. Nature 456(7223):770–772. doi:10.1038/nature07571

Ventura B, Notarnicola C, Casarano D, Posa F, Hayes AG, Wye L (2012) Electromagnetic models and inversion techniques for Titan's Ontario Lacus depth estimation from Cassini RADAR data. Icarus 221(2):960–969. doi:10.1016/j.icarus.2012.09.011

Volkov VA, Johannessen OM, Borodachev VE, Voinov GN, Pettersson LH, Bobylev LP, Kouraev AV (2002) Polar seas oceanography: an integrated case study of the Kara Sea. Springer Science & Business Media

Wall S, Hayes AG, Bristow C, Lorenz RD, Stofan ER, Lunine JI, Le Gall A, Janssen M, Lopes R, Wye L et al (2010) Active shoreline of Ontario Lacus, Titan: a morphological study of the lake and its surroundings. Geophys Res Lett 37(5):L05,202. doi:10.1029/2009GL041821